## General Disclaimer

## One or more of the Following Statements may affect this Document

- This document has been reproduced from the best copy furnished by the organizational source. It is being released in the interest of making available as much information as possible.

- This document may contain data, which exceeds the sheet parameters. It was furnished in this condition by the organizational source and is the best copy available.

- This document may contain tone-on-tone or color graphs, charts and/or pictures, which have been reproduced in black and white.

- This document is paginated as submitted by the original source.

- Portions of this document are not fully legible due to the historical nature of some of the material. However, it is the best reproduction available from the original submission.

NSG-1414



HOWARD UNIVERSITY
SCHOOL OF ENGINEERINC
DEPARTMENT OF MECHANICAL ENGINEERING
WASHINGTON, D.C. 20059

FINAL REPORT

NASA GRANT: NSG 1414, Suppl. 7

# THE DYNAMICS AND CONTROL OF LARGE FLEXIBLE SPACE STRUCTURES - VIII

by

Peter M. Bainum
Professor of Aerospace Engineering
Principal Investigator

and

A.S.S.R. Reddy
Assistant Professor
Co-Investigator

and

Cheick M. Diarra and S. Ananthakrishnan

Graduate Research Assistants

June 1985

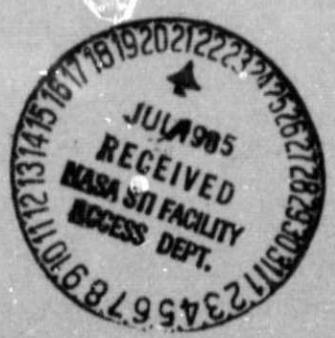

HOWARD UNIVERSITY
SCHOOL OF ENGINEERING
DEPARTMENT OF MECHANICAL ENGINEERING
WASHINGTON, D.C. 20059

FINAL REPORT

NASA GRANT: NSG-1414, Suppl. 7

# THE DYNAMICS AND CONTROL OF LARGE FLEXIBLE SPACE STRUCTURES-VIII

by

Peter M. Bainum
Professor of Aerospace Engineering
Principal Investigator

and

A.S.S.R. Reddy
Assistant Professor
Co-Investigator

and

Cheick M. Diarra and S. Ananthakrishnan

Graduate Research Assistants

June 1985

## ABSTRACT

A development of the in-plane open-loop rotational equations of motion for the proposed SCOLE in-orbit configuration is presented based on an Eulerian formulation. The mast is considered to be a flexible beam connected to the (rigid) Shuttle and the reflector. Frequencies and mode shapes are obtained for the mast vibrational appendage modes (assumed to be decoupled) for different boundary conditions based on continuum approaches and also preliminary results are obtained using a finite element representation of the mast-reflector sytem. The linearized rotational in-plane equation is characterized by periodic coefficients and open-loop system stability can be examined with an application of the Floquet theorem. Numerical results are presented to illustrate the potential instability associated with actuator time delays even for delays which represent only a small fraction of the natural period of oscillation of the modes contained in the open-loop model of the system. When plant and measurement noise effects are added to the previously designed deterministic model of the Hoop/Column system, it is seen that both the system transient and steady state performance are degraded. Mission requirements can be satisfied by appropriate assignment of cost function weighting elements and changes in the ratio of plant noise to measurement noise.

TABLE OF CONTENTS

LIST OF FIGURES

# I. INTRODUCTION

The present grant extends the research effort initiated in previous grant years (May 1977 - Feb. 1984) and reported in Refs. 1-10*. Techniques for controlling both the attitude and shape of very large inherently flexible proposed future spacecraft systems are being studied. Suggested applications of such large systems in orbit include: large scale multi-beam antenna systems; earth observation and resource sensing systems; orbitally based electronic mail transmission; and as in-orbit test models designed to compare the performance of flexible systems with that predicted based on computer simulations and/or on scale model Earth-based laboratory experiments.

This report is subdivided into five chapters. Chapter II begins with a preliminary development of a two dimensional model of the rotational equations of motion for the proposed Spacecraft Control Laboratory Experiment - SCOLE[11], correcting some inconsistencies contained in a similar development appearing in last year's final grant report[10]. This development is based on the expansion of the Eulerian moment equations assuming that the Shuttle and the reflector are rigid bodies, and modelling the mast as a connecting flexible beam. Calculations are then performed to obtain the frequencies of the fundamental and subsequent bending and torsional modes as well as examples of the corresponding modal shape functions. Bending modal frequencies are calculated based on different assumed boundary conditions: (1) where the flexible mast is modelled as a cantilever attached to the Shuttle end such that the displacement and slope at the Shuttle attachment point are zero; (2) where the mast is considered as a flexible beam accounting for the rotational inertia of both the Shuttle

*References cited in this report are listed separately at the end of each chapter.

and the reflector as end bodies. The cases of in-plane and out-of-plane bending are treated as separate decoupled motions. Frequencies are also approximated through a preliminary application of the STRUDL finite element algorithm where the reflector as well as the mast are assumed to be constructed of the same material. A comparison can then be made with the previous NASA results[11] and preliminary results presented by the Harris Corp. in the SCOLE Workshop[12] held at Langley during December 1984. Finally, Chapter II commences with a preliminary stability analysis of the open-loop in-plane SCOLE dynamics based on an application of Floquet's theorem. Analytical results can be obtained for two special cases: (1) where the offset of the mast attachment point on the reflector is set to zero; and (2) where the gravity-gradient torques are not included, but the reflector attachment offset can be non-zero.

In the following chapter the preliminary review of stability techniques that can be applied when time delays are present in the implementation of control inputs, presented in last year's report, is now extended to include representative numerical results. Examples considered include a second order controlled harmonic oscillator system and a fifth order system based on the dynamic model of the F-100 turbofan engine. These examples illustrate the potential instability which could result even for delays which represent only a small fraction of the period of natural oscillation of the various modes in the uncontrolled system.

Chapter IV is based on a paper to be presented at the Fifth VPI & SU/AIAA Symposium on Dynamics and Control of Large Structures and extends work previously initiated during the 1982-1983 grant year and partially supported during the Summer of 1983 on this grant. The evaluation of the

expected performance of the Hoop/Column antenna system subjected to stochastic inputs is now extended to include simulation of the steady state RMS errors in addition to the transient dynamics previously reported (Chapter VI of Ref. 10). The Kalman filter algorithm of the ORACLS[13] package is used to develop control laws and simulate the estimate of the state in an optimal LQG fashion. The results of Ref. 10 are also extended here to include the effects of non co-location of actuators and/or sensors. As a specific example the actuator (or the sensor) assumed to be mounted on the hoop assembly is then removed to examine the projected effects on the transient, steady state (RMS) errors, and the estimator performance.

Chapter V describes the main general conclusions together with future recommendations. The effort described in Chapters II and III is being continued during the 1985-86 grant period in accordance with our proposal[14] and subsequent discussions.

## References


1. Bainum, P.M. and Sellappan, R., "The Dynamics and Control of Large Flexible Space Structures," Final Report NASA Grant: NSG-1414, Part A: Discrete Model and Modal Control, Howard University, May 1978.

2. Bainum, Peter M., Kumar, V.K., and James, Paul K., "The Dynamics and Control of Large Flexible Space Structures," Final Report, NASA Grant: NSG-1414, Part B: Development of Continuum Model and Computer Simulation, Howard University, May 1978.

3. Bainum, P.M. and Reddy, A.S.S.R., "The Dynamics and Control of Large Flexible Space Structures II," Final Report, NASA Grant NSG-1414, Suppl. I, Part A: Shape and Orientation Control Using Point Actuators, Howard University, June 1979.

4. Bainum, P.M., James, P.K., Krishna, R., and Kumar, V.K., "The Dynamics and Control of Large Flexible Space Structures II," Final Report, NASA Grant NSG-1414, Suppl. 1, Part B: Model Development and Computer Simulation, Howard University, June 1979.

5. Bainum, P.M., Krishna, R., and James, P.K., "The Dynamics and Control of Large Flexible Space Structures III," Final Report, NASA Grant NSG-1414, Suppl. 2, Part A: Shape and Orientation Control of a Platform in Orbit Using Point Actuators, Howard University, June 1980.

6. Bainum, P.M. and Kumar, V.K., "The Dynamics and Control of Large Flexible Space Structures III," Final Report, NASA Grant NSG-1414, Suppl. 2, Part B: The Modelling, Dynamics and Stability of Large Earth Pointing Orbiting Structures, Howard University, September 1980.

7. Bainum, P.M., Kumar, V.K., Krishna, R. and Reddy, A.S.S.R., "The Dynamics and Control of Large Flexible Space Structures IV," Final Report, NASA Grant NSG-1414, Suppl. 3, NASA CR-165815, Howard University, August 1981.

8. Bainum, P.M., Reddy, A.S.S.R., Krishna, R., Diarra, C.M., and Kumar, V.K., "The Dynamics and Control of Large Flexible Space Structures V", Final Report, NASA Grant NSG-1414, Suppl. 4, NASA CR-169360, Howard University, August 1982.

9. Bainum, P.M., Reddy, A.S.S.R., Krishna, R., and Diarra, C.M., "The Dynamics and Control of Large Flexible Space Structures VI," Final Report NASA Grant NSG-1414, Suppl. 5, Howard University, Sept. 1983.

10. Bainum, P.M., Reddy, A.S.S.R., Krishna, R., Diarra, C.M. and Ananthakrishnan, S., "The Dynamics and Control of Large Flexible Space Structures-VII," Final Report NASA Grant NSG-1414, Suppl 6, Howard University, June 1984.

11. Taylor, L.W. and Balakrishnan, A.V., "A Mathematical Problem and a Spacecraft Control Laboratory Experiment (SCOLE) Used to Evaluate Control Laws for Flexible Spacecraft ... NASA/IEEE Design Challenge," (Rev.), January 1984. (originally presented at AIAA/VPI&SU Symposium on Dynamics and Control of Large Structures, June 6-8, 1983).

12. Proceedings of the SCOLE Workshop, NASA Langley Research Center, Hampton, Va., Dec. 6-7, 1984 (compiled by Larry Taylor).

13. Armstrong, E.S., "ORACLS - A System for Linear Quadratic-Gaussian Control Law Design," NASA Technical Paper 1106, April 1978.

14. Bainum, P.M. and Reddy, A.S.S.R., "Proposal for Research Grant on: 'The Dynamics and Control of Large Flexible Space Structures IX,'" Howard University (submitted to NASA), October 15, 1984.

# II. MODELLING TECHNIQUES FOR THE SPACECRAFT CONTROL LABORATORY EXPERIMENT

The transfer of large, massive payloads into Earth orbit is currently accomplished with considerable propulsive and control effort. As a result, spacecraft designers must strive to minimize a large structure's mass. Consequently, many of the future spacecraft will be very flexible and will require that their shape and orientation be controlled.[1] The problem of controlling large, flexible space systems has been the subject of considerable research. Many approaches to control system synthesis have been evaluated using computer simulations including a preliminary synthesis of control laws for the proposed Hoop/Column System.[2,3] Ground experiments have also been used to validate system performance under more realistic conditions but based on simple structures such as beams and plates.[4] In a recent paper, SCOLE (Spacecraft Control Laboratory Experiment), Lawrence W. Taylor Jr. and A.V. Balakrishnan described a proposed laboratory experiment based on a model of the Shuttle connected to a flexible beam with a reflecting grillage mounted at the end of the beam[5] (Fig. 2.1). The authors stressed the need to directly compare competing control design techniques, and discussed the feasibility of such direct comparison. Concern would be given to modelling order reduction, fault management, stability, and dynamic system performance.

With this paper[5] as a background, the purpose of the study proposed here is to model the system in different phases where each successive phase would represent a mathematical model successively closer to that of the actual laboratory system.

It is anticipated that this (multi-year) study would consist of five parts, the first of which would consist of a literature survey during which the investigators would familiarize themselves with different mathematical modelling techniques.

During the second part, the system would be successively modelled as follows:

a) The Space Shuttle as a rigid body; the reflector mast as a flexible beam type appendage; and the reflector as a rigid plate. The mast shape functions are actually solved from the fourth order non-linear flexural beam equation with different boundary conditions imposed on both the Shuttle and grillage ends. b) Here the Space Shuttle would be treated as a rigid body body; the composite appendage consisting of the flexible reflector mast and also the continuous rigid reflector (grillage) could be modelled using finite element techniques. Then the composite system dynamics can be modelled using the hybrid coordinate technique[6] which involves sets of matrix equations describing the motion of the main vehicle as well as that of any attached appendages. It is anticipated that within the second part of this study these different mathematical models would be developed in a form suitable for numerical simulation.

During the third part, each of these models could be directly compared with the model proposed in the SCOLE paper[5], beginning with the simulation of the open-loop system dynamics. The fourth part of the effort would consist of the control law synthesis when the model can be described by linear system dynamics - i.e., in response to small perturbations induced on the system about the nominal laboratory configuration and orientation, or after a major slewing maneuver, to remove the

remaining transients which exist in a neighborhood of the new equilibrium orientation. Such a construction of control laws will probably be based on the ORACLS software package.[7] Strategies would be developed to control the shape and orientation of the beam/grillage.

First the controllability of the system could be examined based on the graph theoretic techniques already employed for a similar analysis of the Hoop/Column system[3], for different combinations of numbers and locations of the actuators. Next, control laws can be constructed based on the techniques of optimal control theory, and studies can be performed comparing transient and control effort characteristics for a variety of system parameters and weighting matrix elements.

Finally, the fifth part would focus on the slewing maneuvers to accurately point the reflector at a specific target in a minimum lapse of time. For simple maneuvers (single axis) attempts would be made to analytically determine the slewing control law; for more general maneuvers, numerical techniques would be implemented.

II. A Development of the Two Dimensional Model - (Eulerian Moment Equations)

The SCOLE system is assumed to be comprised of three main parts (Fig. 2.1):

i) the Space Shuttle Orbiter with its center of mass located at point $O_1$;

ii) the mast, treated as a 130 ft long beam, connected to the Shuttle at $O_2$ and to the reflector at $O_3$;

iii) the reflector, considered to be a flat plate with its center of mass at $O_4$.

The preliminary analysis presented here started before it was specified[8] that the interface point between the mast and the Shuttle is at $O_1$.[8] Therefore, in what follows, a position vector $\vec{R}_1$ appears which defines $\vec{O_1O_2}$, where $O_2$ is the assumed interface point.

In the following analysis, the angular momentum of the entire system is evaluated at point $O_1$ and the dynamics include the lateral displacements of the beam.

II. A.1 Angular Momentum of the Shuttle with Respect to Point $O_1$

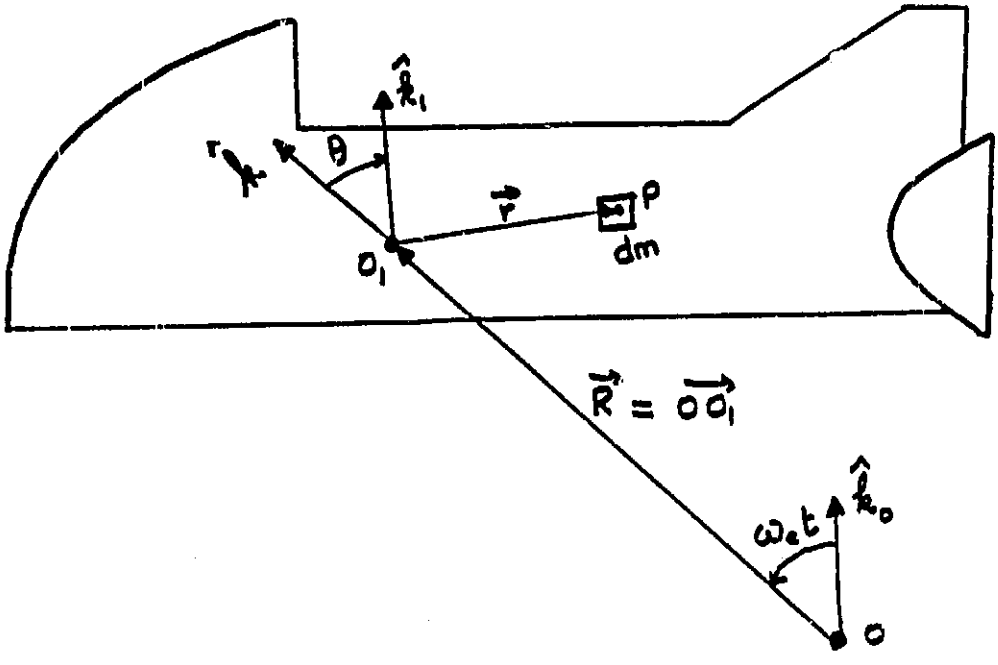

Consider a point, P, of mass, dm, at an arbitrary position in the Shuttle such that $\vec{O_1P} = \vec{r}$. The elemental angular momentum of the mass, dm, is given by:

$$d\vec{H}_{O_1} = \vec{r} \times \frac{d}{dt}\vec{OP}\Big|_{R_o} dm = \vec{r} \times \frac{d}{dt}(\vec{R}+\vec{r})\Big|_{R_o} dm$$
$$= \vec{r} \times \{\dot{R}\hat{k} + R\omega_c \hat{\imath} + (\omega_c - \dot{\theta})\hat{\jmath} \times \vec{r}\}\, dm \qquad (2.1)$$

The total angular momentum for the Shuttle is obtained by integrating Eq. (2.1) over the entire mass of Shuttle as:

$$\vec{H}_{S_{O_1}} = -\dot{R}\hat{k} \times \int_{M_s} \vec{r}\, dm - R\omega_c \hat{\imath} \times \int_{M_s} \vec{r}\, dm + \int_{M_s} \vec{r} \times \{(\omega_c - \dot{\theta})\hat{\jmath} \times \vec{r}\}\, dm \qquad (2.2)$$

The first and second integrals appearing in the right side of Eq. (2.2) vanish because the center of mass of the Shuttle is at point $O_1$.

Since $\vec{r} \cdot \hat{\jmath} = 0$, Eq. (2.2) takes the form:

$$\vec{H}_{S/O_1} = (\omega_c - \dot{\theta})\hat{\jmath} \int_{M_s} r^2\, dm = \mathrm{II}_s\, \vec{\omega}_{R_1/R_o} \qquad (2.3)$$

where $\mathrm{II}_s$ is the Inertia tensor of the Shuttle at point $O_1$ and $\vec{\omega}_{R_1/R_0} = (\omega_c - \dot{\theta})\,\hat{\jmath}$.

II. A.2 Angular Momentum of the Mast with Respect to Point $O_1$

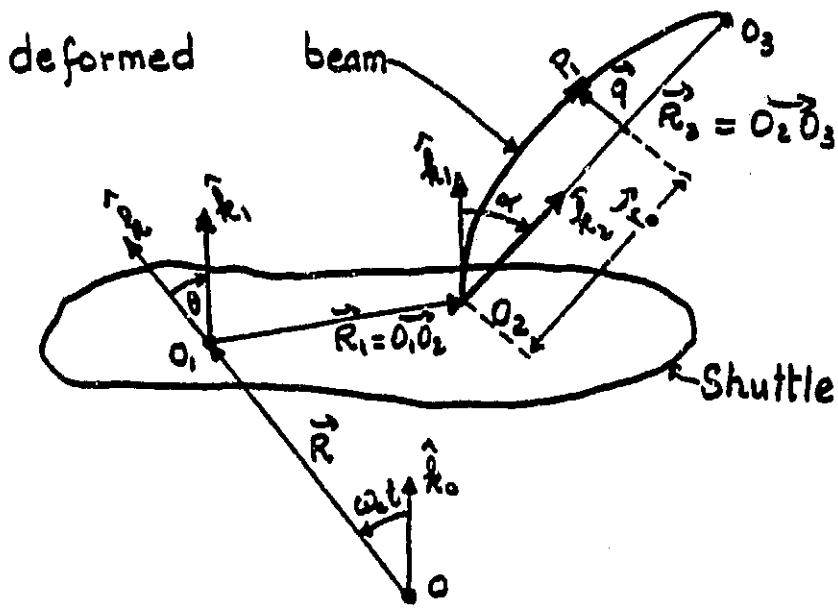

Consider here an element of the mast located at point, $P_1$, with mass, dm. The elemental angular momentum of such an element is given by:

$$\underline{d\vec{H}}_{M/O_1} = \left\{ \overrightarrow{O_1P_1} \times \frac{d}{dt} \overrightarrow{QP_1}/R_o \right\} dm \tag{2.4}$$

if one notes that

$$\begin{aligned} \overrightarrow{O_1P_1} &= \vec{r}_o + \vec{q} \\ \overrightarrow{OP_1} &= \vec{R} + \vec{r}_o + \vec{q} \end{aligned} \tag{2.5}$$

then, Eq. (2.4) may be expanded according to:

$$\vec{H}_{M/O_1} = -\frac{d\vec{R}}{dt}/R_o \times \int_{M_m} (r_o \hat{k}_2 + q\hat{i}_2)\, dm + \int_{M_m} (r_o k_2 + q i_2) \times (\dot{r}_o \hat{k}_2 + \dot{q}\hat{i}_2)\, dm \tag{2.6}$$

$\frac{d\vec{R}}{dt}/R_o$ is expressed using the relationship between the rate of change of a vector, $\vec{w}$, in an inertial ($R_o$) and rotating ($R_1$) frames, i.e.

$$\frac{d}{dt}\vec{w}/R_o = \frac{d}{dt}\vec{w}/R_i + \vec{\Omega}_{R_i/R_o} \times \vec{w} \tag{2.7}$$

After substitution of Eq. (2.7) into Eq. (2.6) and integration term by term, one can develop:

$$\begin{aligned} \vec{H}_{M/O_1} = M_m \Big[ & \omega_c R \Big[ \cos(\alpha+\theta)\frac{l}{2} + \sin(\alpha+\theta)\Big\{ \frac{\alpha l}{2} \\ & - \frac{1}{\beta l}\cos(\omega t+\phi)(A\sin\beta l - B\cos\beta l + C\sinh\beta l + D\cosh\beta l + B - D)\Big\}\Big] \\ & + \dot{\alpha}\frac{l^2}{3} + \omega\sin(\omega t+\phi)\Big\{ \frac{1}{\beta}(A\sin\beta l - B\cos\beta l + C\sinh\beta l + D\cosh\beta l) \\ & + \frac{1}{\beta^2 l}(A\cos\beta l + B\sin\beta l - C\cosh\beta l - D\sinh\beta l - A + C)\Big\} + \frac{l^2}{3}(\omega_c - \dot{\theta} - \dot{\alpha})\Big] \hat{j} \end{aligned} \tag{2.8}$$

If $q(x,t)$ is assumed $= A\cos\beta x + B\sin\beta x + C\cosh\beta l + D\sinh\beta x$

II. A.3 Angular Momentum of the Rigid Reflector with Respect to Point $O_1$

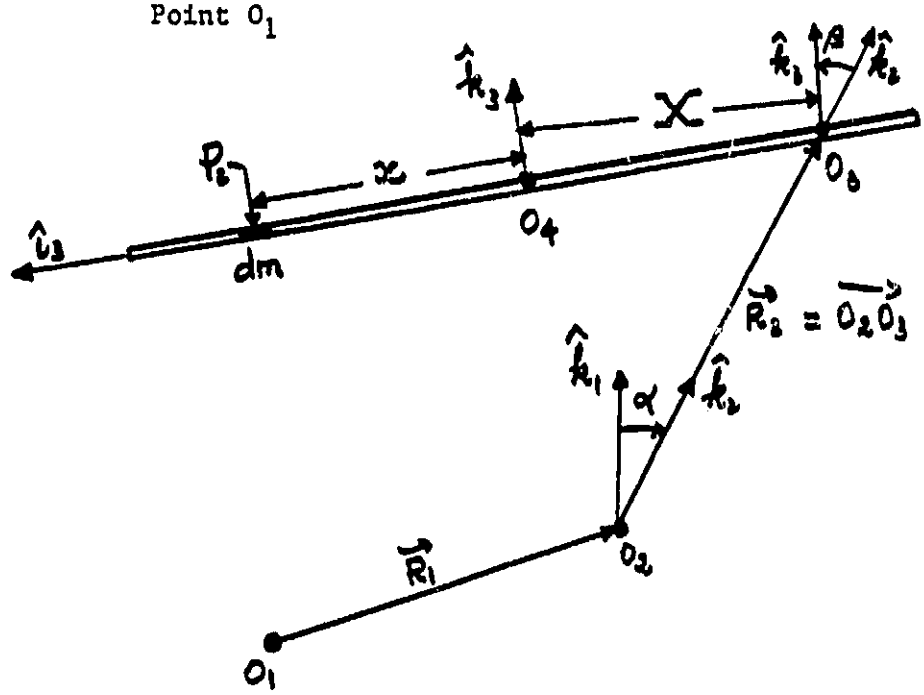


Let $O_4$ be the center of mass of the reflector, and $O_3$ the interface point between the reflector and the mast. The distance, X, between $O_3$ and $O_4$ is constant since the reflector is assumed to be rigid, at least for this analysis.

Let us now consider an element of mass, dm, of the reflector located at an arbitrary point, $P_2$. The elemental angular momentum of that element of mass can be expressed as:

$$d\vec{H}_{r/O_1} = \overrightarrow{O_1P_2} \times \frac{d}{dt}(\overrightarrow{OP_2})\Big|_{\mathcal{R}_0} dm \qquad (2.9)$$

$\vec{O_1P_2}$ and $\vec{O_2P_2}$ can be expressed as:

$$\left.\begin{aligned} \overrightarrow{O_1P_2} &= \vec{R}_1 + \vec{R}_2 + X\hat{\imath}_3 + x\hat{\imath}_3 \\ \overrightarrow{OP_2} &= \vec{R} + \overrightarrow{O_1P_2} \end{aligned}\right\} (2.10)$$

Eq. (2.9) may be expanded according to

$$d\vec{H}_{r/O_1} = \left(\vec{R}_1 + (X+x)\hat{i}_3\right) \times \frac{d}{dt}\left[\vec{R} + \vec{R}_2 + (X+x)\hat{i}_3\right]/R_O \qquad (2.11)$$

Once more, $\frac{d}{dt}\left[\vec{R} + \vec{R}_2 + (X+x)\hat{i}_3\right]/R_O$ is expressed using Eq. (2.7):

$$\frac{d}{dt}\vec{w}/R_O = \frac{d}{dt}\vec{w}/R_i + \vec{\Omega}R_i/R_O \times \vec{w}$$

After substitution of Eq. (2.7) into Eq. (2.11) and integration term by term over the entire mass of the reflector, one arrives at

$$\vec{H}_{r/O_1} = \int M_r R R_2 \omega_c \cos(\alpha+\theta) + M_r X R \omega_c \times \sin(\alpha+\theta) + \left(\omega_c - \dot{\theta} - \dot{\alpha}\right)\left[I_{2r} + M_r\left(X^2 + R_2^2\right)\right]\hat{j} \qquad (2.12)$$

where $I_{2r}$ is the moment of inertia of the reflector about the $\hat{j}$ axis taken at point $O_4$.

II. B.1 Moment Equation

The angular momentum of the entire system about $0_1$ is obtained by summing the angular momentum of each part about $0_1$, i.e.

$$\vec{H}_{T/0_1} = \sum_{i=1}^{3} \vec{H}_{i/0_1} \tag{2.13}$$

The moment equation

$$\frac{d}{dt} \vec{H}_{T/0_1/R_0} = \vec{N} \tag{2.14}$$

where N is the sum of all the external torques, acting on the entire system, about an axis through point $0_1$.

At this stage of the analysis, it is assumed that the center of mass of the Shuttle moves in a circular orbit, i.e.

$$\frac{d}{dt} \vec{R}_{/R} = \dot{\vec{R}}_{/R} = \vec{0} \tag{2.15}$$

Taking into consideration the coincidence between points $0_1$ and $0_2$, Eq. (2.14) is expanded using once more Eq. (2.7) and the following result is obtained:

$$\frac{d}{dt} \vec{H}_{T/0_1/R_0} \cdot \hat{j} = \vec{N} \cdot \hat{j} = N_y =$$

$$- \ddot{\theta} \left( I_{2S} + M_m \frac{\ell^2}{3} + I_{Sr} + M_r (X^2 + R_2^2) \right)$$

$$- \ddot{\alpha} \left( I_{2r} + M_r (X^2 + R_2^2) \right) + (\alpha + \theta) \dot{\alpha} \frac{\ell}{2} M_m \omega_c R$$

$$+ (\dot{\theta} + \dot{\alpha}) \left\{ M_m \left[ \omega_c R \left\{ (\theta + \alpha) \frac{\ell}{2} + \frac{\alpha \ell}{2} - \frac{1}{B\ell} \cos(\omega t + \phi) \right\} \right. \right. x$$

$$(A\sin\beta\ell - B\cos\beta\ell + C\sinh\beta\ell + D\cosh\beta\ell + B - D)\}]$$

$$- M_r (R R_2 \omega_c (\theta+\alpha) + \dot{X} R \omega_c)\}$$

$$+ M_m \omega_c R\left[(\alpha+\theta)\frac{\omega}{\beta\ell}\sin(\omega t+\phi)(A\sin\beta\ell\right.$$

$$\left. - B\cos\beta\ell + C\sinh\beta\ell + D\cosh\beta\ell + B - D)\right]$$

$$+ M_m \omega^2 \cos(\omega t+\phi)\left\{\frac{1}{\beta\ell}(A\sin\beta\ell + C\sinh\beta\ell - B\cos\beta\ell\right.$$

$$\left. + D\cosh\beta\ell) + \frac{1}{\beta^2\ell}(A\cos\beta\ell + B\sin\beta\ell - C\cosh\beta\ell\right.$$

$$\left. - D\sinh\beta\ell - A + C\right\}$$

But

$$\alpha = \frac{1}{\ell}\cos(\omega t+\phi)\psi(\ell)$$

$$\dot{\alpha} = -\frac{\omega}{\ell}\sin(\omega t+\phi)\psi(\ell)$$

$$\ddot{\alpha} = -\frac{\omega^2}{\ell}\cos(\omega t+\phi)\psi(\ell)$$

(2.16)

II. B.2 Expression for $\vec{q}$

In the moment equation, Eq. (2.16), one notices integrals involving $\vec{q}$, the transverse displacement vector, and its first and and second derivatives with respect to time. It is, therefore, necessary to develop an expression for $\vec{q}$.

II.B.2.i Relation between q(x,t) and y(x,t)

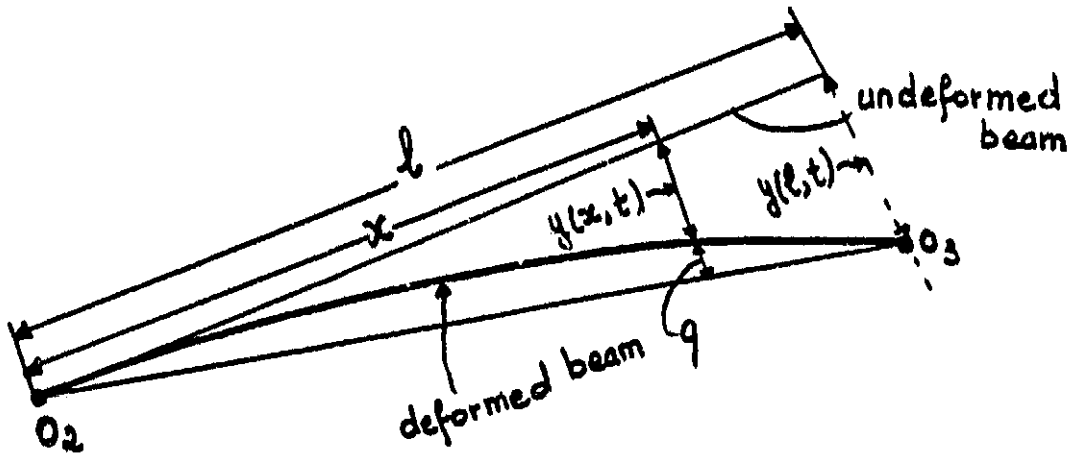


Consider the beam in its deflected configuration. $y(\ell,t)$ is the deflection of the reflector-end of the mast at an arbitrary time, t; $y(x,t)$, the deflection of an arbitrary point on the mast at the same time.

From Fig. (2.1), $\hat{k}_1 \cdot \hat{k}_2 = \cos\alpha$ (2.17)

Assuming $\alpha$ small, $\tan\alpha$ can be expressed as

$$\tan\alpha = \frac{y(\ell,t)}{\ell} \approx \alpha = \frac{y(x,t)+q(x,t)}{x} \qquad (2.18)$$

From Eq. (2.18) one derives

$$q(x,t) = \frac{x\, y(\ell,t)}{\ell} - y(x,t) \tag{2.19}$$

or

$$q(x,t) = \alpha x - y(x,t) \tag{2.20}$$

II.B.2.ii Evaluation of y(x,t)

Assuming separability of the variables, the beam equation,

$$+\frac{EI}{\rho A}\frac{\partial^4 y(x,t)}{\partial x^4} + \frac{\partial^2 y(x,t)}{\partial t^2} = 0 \tag{2.21}$$

is solved to yield solutions of the form:

$$y(x,t) = f(t)\,\phi(x) \tag{2.22}$$

where

$f(t)$ = E sinωt + F cosωt with ω = frequency of the vibration

and $\phi(x)$ = A cosβx + B sinβx + C coshβx + D sinhβx (2.23)

When the following boundary conditions are assumed:

a) $y(0,t) = 0$ ; b) $y'(0,t) = 0$

c) $EI\, y'''(\ell,t) = -Mr\, \ddot{y}(\ell,t)$; d) $EI\, y''(\ell,t) = 0$ (2.24)

where $y' = \frac{\partial y}{\partial x}$ and $\dot{y} = \frac{\partial y}{\partial t}$ (2.25)

these can be expressed in the form:

$$\left.\begin{aligned} \alpha A + \delta B &= 0 \\ \gamma A + \Gamma B &= 0 \end{aligned}\right\} \Leftrightarrow \underbrace{\begin{bmatrix} \alpha & \delta \\ \gamma & \Gamma \end{bmatrix}}_{C} \begin{bmatrix} A \\ B \end{bmatrix} = \begin{bmatrix} 0 \\ 0 \end{bmatrix} \tag{2.26}$$

where

$$\alpha = \sin\beta\ell - \sinh\beta\ell - \frac{M_r}{\rho A'}\beta\,(\cos\beta\ell - \cosh\beta\ell)$$

$$\delta = -\cos\beta\ell - \cosh\beta\ell - \frac{M_r}{\rho A'}\beta\,(\sin\beta\ell - \sinh\beta\ell) \qquad (2.26)$$

$$\gamma = \cos\beta\ell + \cosh\beta\ell$$

$$\sigma = \sin\beta\ell + \sinh\beta\ell$$

$$\beta^2 = \omega\sqrt{\frac{\rho A'}{EI}} \qquad (2.28)$$

For the SCOLE system, the following parameters have been supplied[8]:

$\rho A' = 0.09556$ slugs/ft

$EI = 4.0\times10^7$ lb-ft$^2$

$M_r = (400/32.2)$ slugs

$\ell = 130$ ft.

For non-trivial solutions for A and B, det C must vanish. The values of $\beta$ for which det C = 0 are computed and substituted back into Eq. (2.28) to obtain the frequencies of the different vibrational modes (Table 2.1).

The same values of $\beta$ are substituted into $\phi(x)$, (Eq. 2.23), which is normalized with respect to its maximum value and the normalized mode shapes plotted (see Table 2.1 and Figs. 2.2 - 2.6). Note that the ranges of frequencies obtained in Table 2.1 are higher then those prevously presented in the April 13, 1984 oral presentation due to previous inconsistencies in dimensional analysis of some physical units.

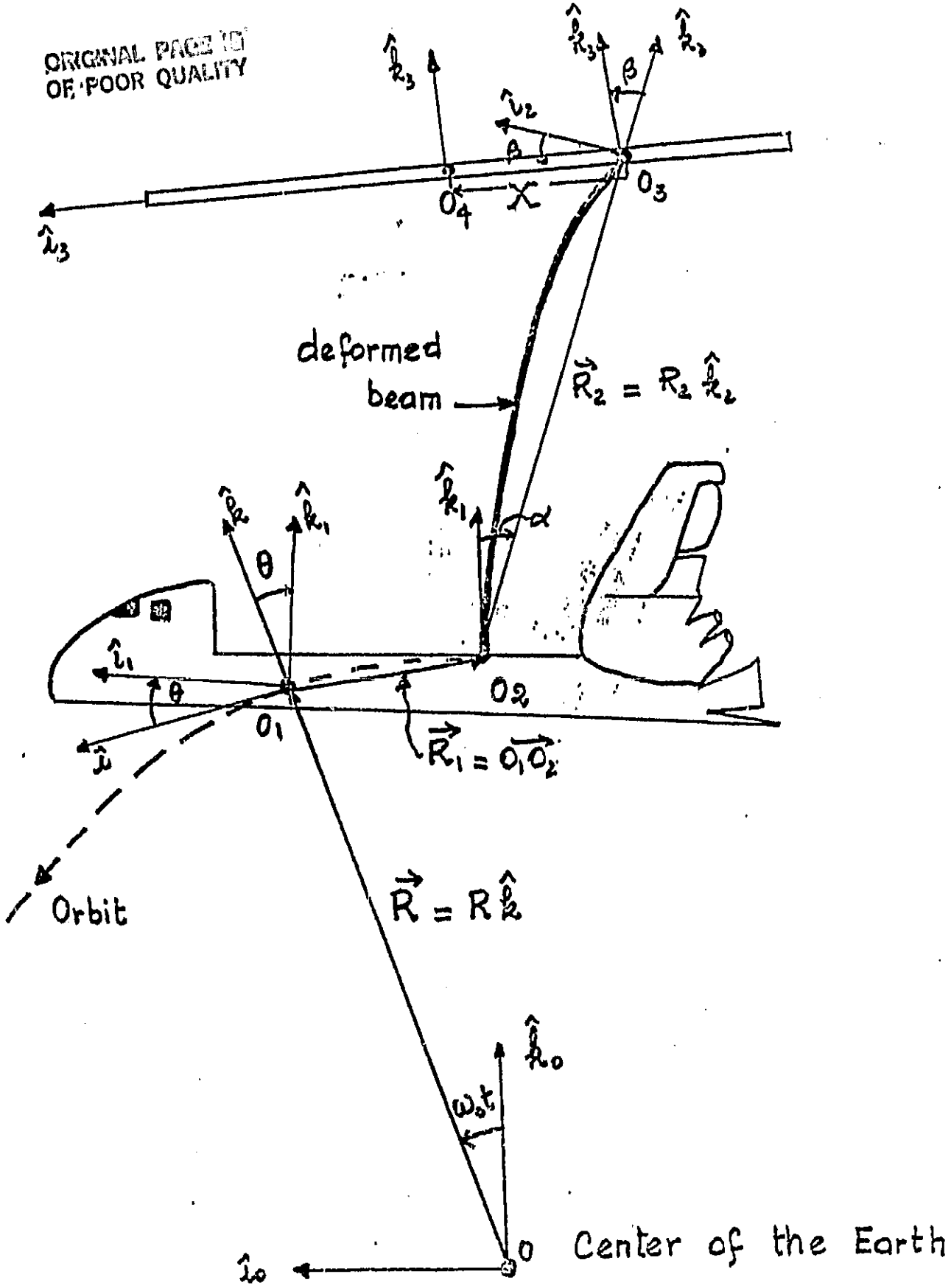


Fig. 2.1. SCOLE System Geometry in the Deformed State (2-D)

TABLE 2.1

Values of β and Natural Frequencies (HZ)
for the First 8 In-Plane (Pitch) Bending Modes

| β | ω(Hz) |
|---|---|
| 1.874599 | .677828 |
| 4.6929 | 4.245 |
| 7.8519 | 11.884 |
| 10.997 | 23.3128 |
| 14.1309 | 38.4933 |
| 17.276 | 57.5283 |
| 20.4229 | 80.4045 |
| 23.555 | 106.958 |

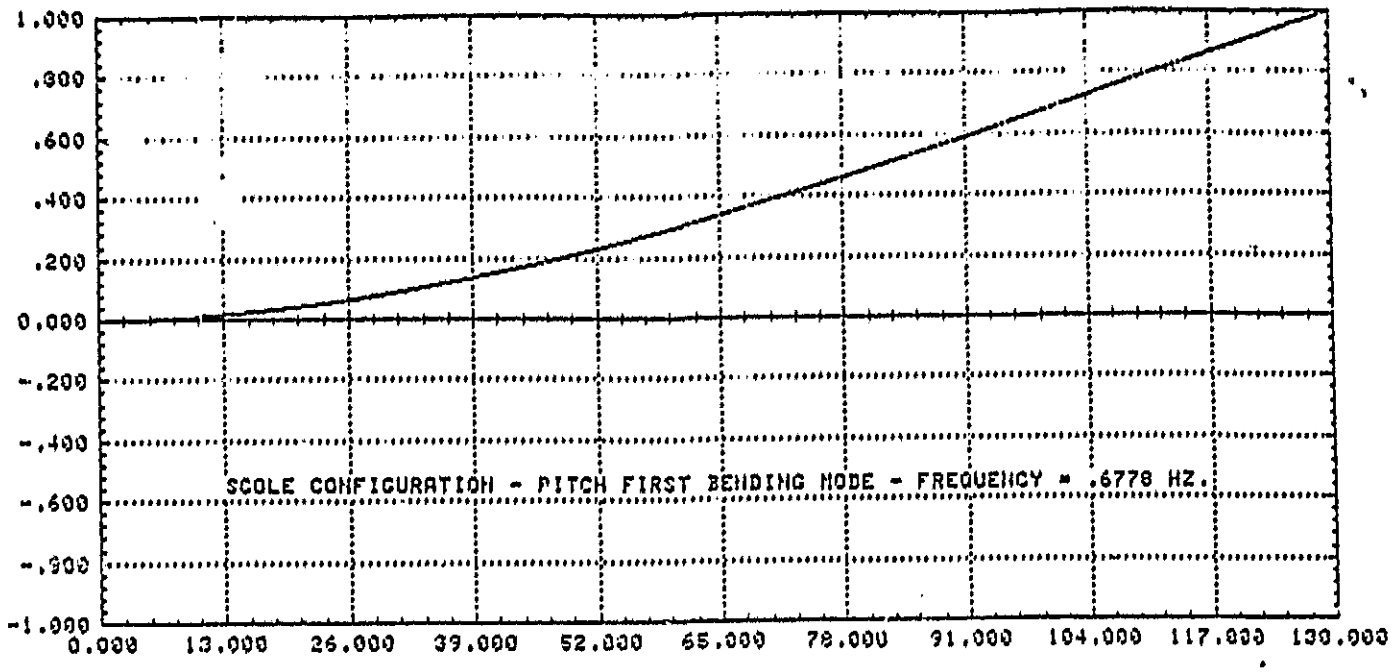
1.000
.800
.600
.400
.200
0.000
-.200
-.400
-.600
-.800
-1.000
SCALE CONFIGURATION - PITCH FIRST BENDING MODE - FREQUENCY = .6778 HZ.
0.000
13.000
26.000
39.000
52.000
65.000
78.000
91.000
104.000
117.000
130.000

Fig. 2.2

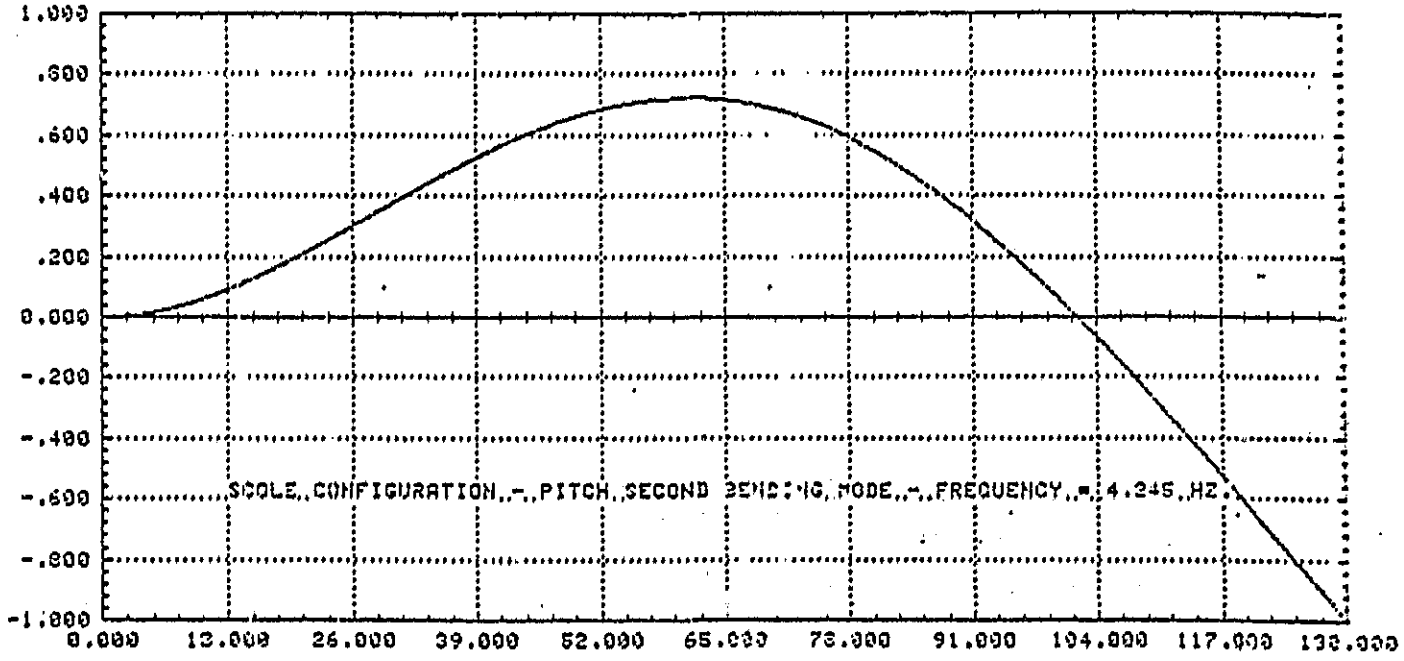
1.000
.800
.600
.400
.200
0.000
-.200
-.400
-.600
-.800
-1.000
SCALE CONFIGURATION - PITCH SECOND BENDING MODE - FREQUENCY = 4.245 HZ.
0.000
13.000
26.000
39.000
52.000
65.000
78.000
91.000
104.000
117.000
130.000

Fig. 2.3

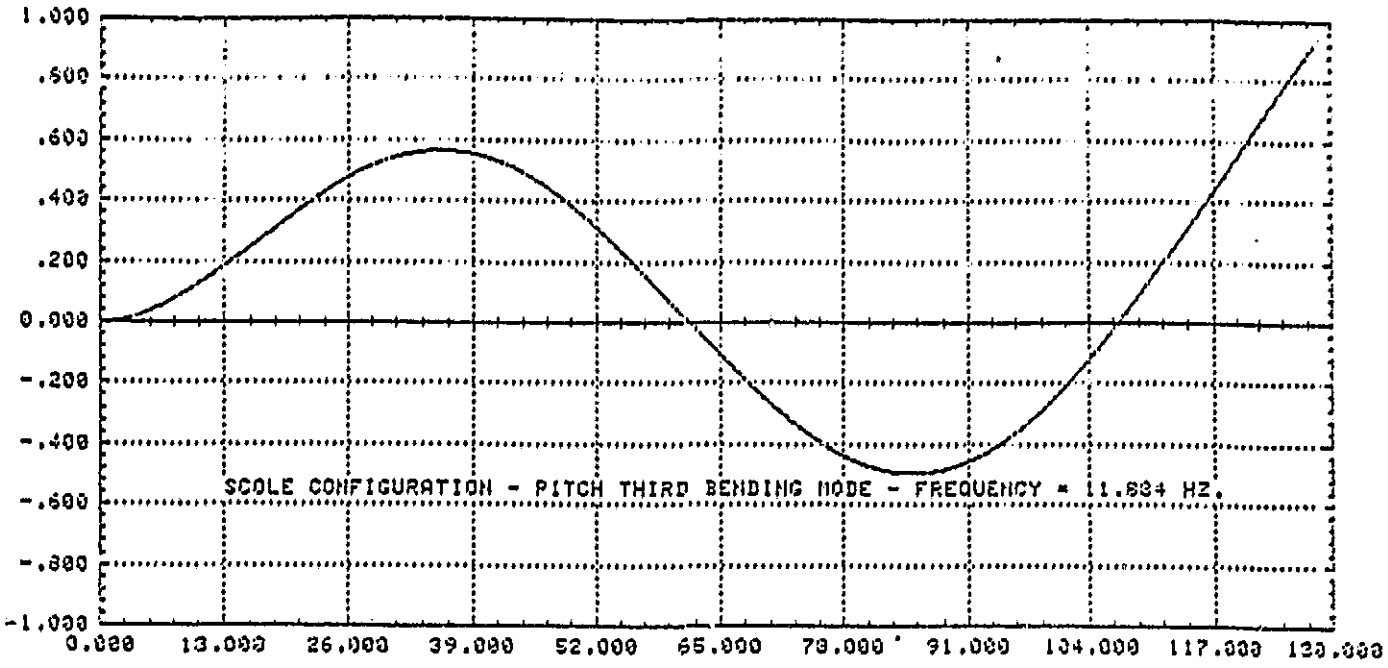
1.000
.800
.600
.400
.200
0.000
-.200
-.400
-.600
-.800
-1.000
0.000
13.000
26.000
39.000
52.000
65.000
78.000
91.000
104.000
117.000
130.000
SCALE CONFIGURATION - PITCH THIRD BENDING MODE - FREQUENCY = 11.834 HZ.

Fig. 2.4

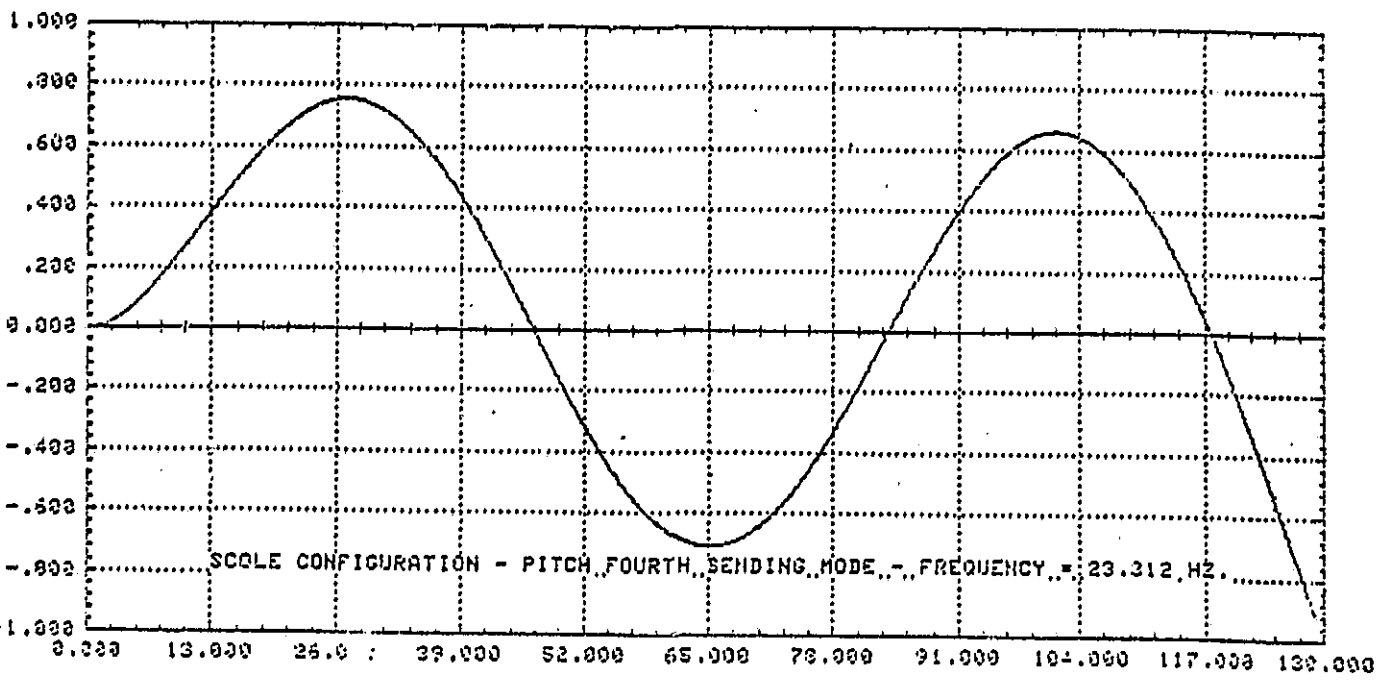
1.000
.800
.600
.400
.200
0.000
-.200
-.400
-.600
-.800
-1.000
13.000
26.0
39.000
52.000
65.000
78.000
91.000
104.000
117.000
130.000
SCALE CONFIGURATION - PITCH FOURTH BENDING MODE - FREQUENCY = 23.312 HZ.

Fig. 2.5

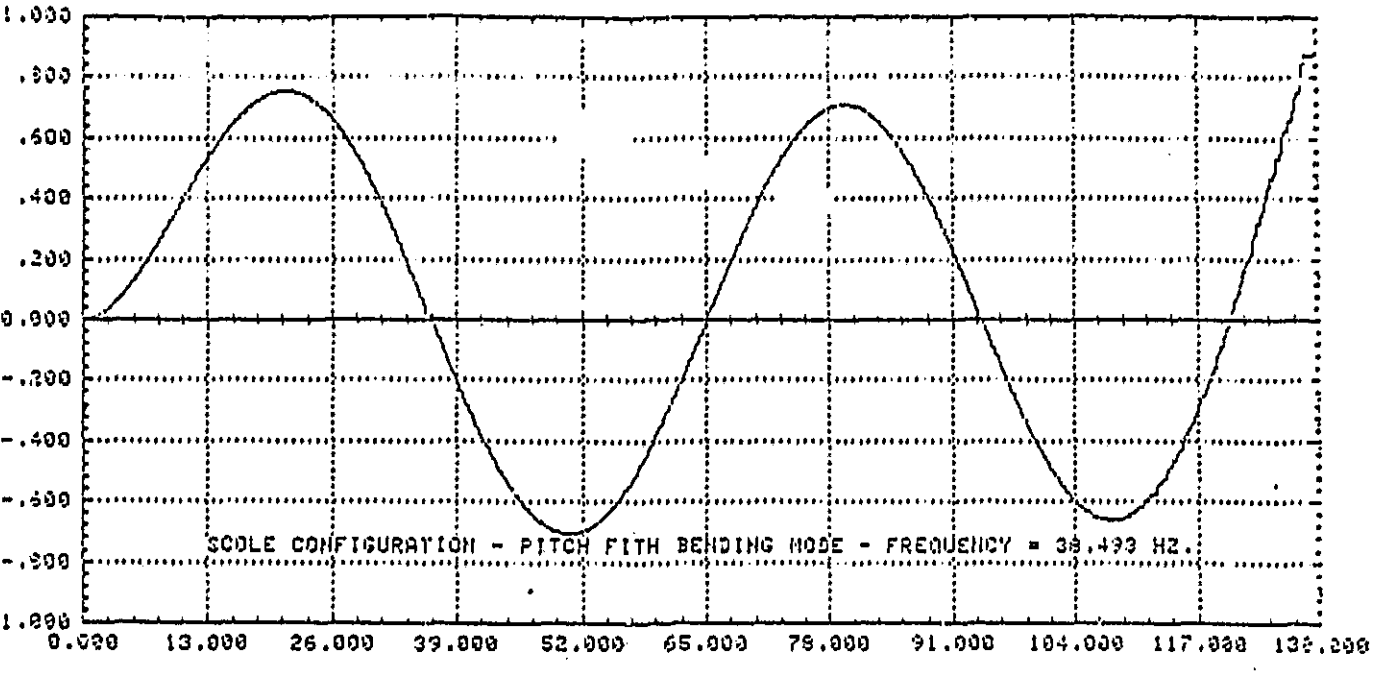


Fig. 2.6

## II.C Frequencies of the Lateral Vibrational Modes when the SCOLE System is Modelled as a Free-Free Beam with End Bodies having Inertia

The solution to the beam equation (2.21) is again considered and the following boundary conditions assumed:

1. The shear force at either end is equal to the mass located at that end multiplied by the acceleration of the interface point at that end.

This boundary condition combined with the equilibrium conditions yields

$$- EI \frac{\partial^3 y(x,t)}{\partial x^3} = M_i \frac{\partial^2 y(x,t)}{\partial t^2}$$

at the Shuttle end,

$$- EI \frac{\partial^3 y(x,t)}{\partial x^3}\Big|_{x=0} = M_s \frac{\partial^2 y(x,t)}{\partial t^2}\Big|_{x=0} = - M_s \omega^2 y(x,t)\Big|_{x=0} \quad (2.29)$$

at the reflector end

$$EI \frac{\partial^3 y(x,t)}{\partial x^3}\Big|_{x=130} = M_r \frac{\partial^2 y(x,t)}{\partial t^2}\Big|_{x=130} = - M_r \omega^2 y(x,t)\Big|_{x=130} \quad (2.30)$$

where

$$\omega^2 = \beta^4 \frac{EI}{\rho A'}$$

2. Next, expressing the equality between the moment at an end point and the product of the inertia of the mass at that end by the angular acceleration of the interface point results in:

$$I_i \ddot{\theta}(x,t) = EI \frac{\partial^2 y(x,t)}{\partial x^2}$$

$$\text{where} \quad \theta(x,t) = \frac{\partial (y(x,t))}{\partial x}.$$

At the Shuttle end: x = 0, this is expressed as:

$$I_s \frac{\partial^2}{\partial t^2} \left[ \frac{\partial y(x,t)}{\partial x} \right]_{x=0} = EI \frac{\partial^2 y(x,t)}{\partial x^2} \Big/_{x=0}$$

$$-\omega^2 I_s \frac{\partial y(x,t)}{\partial x} \Big/_{x=0} = EI \frac{\partial^2 y(x,t)}{\partial x^2} \Big/_{x=0} \qquad (2.31)$$

the same boundary condition at the reflector end translates as:

$$-\omega^2 I_r \frac{\partial y(x,t)}{\partial x} \Big/_{x=130} = -EI \frac{\partial^2 y(x,t)}{\partial x^2} \Big/_{x=130} \qquad (2.32)$$

After performing the required differentiation of the assumed solution of the beam equation (Eq. 2.23), one arrives at the following system of four equations with 4 unknowns, A, B, C, and D,

$$\text{Eq. (2.29)} \Rightarrow \frac{M_s \beta}{\rho A'} A + B + \frac{M_s \beta}{\rho A'} C - D = 0 \qquad (2.33)$$

Eq. (2.30) $\Rightarrow$

$$\left[ \frac{M_r \beta}{\rho A'} \cos \beta l + \sin \beta l \right] A + \left[ \frac{M_r \beta}{\rho A'} \sin \beta l - \cos \beta l \right] B$$

$$+ \left[ \frac{M_r \beta}{\rho A'} \cosh \beta l + \sinh \beta l \right] C + \left[ \frac{M_r \beta}{\rho A'} \sinh \beta l + \cosh \beta l \right] D = 0 \qquad (2.34)$$

Eq. (2.31) $\Rightarrow$

$$-A + \frac{I_s \beta^3}{\rho A'} B + C + \frac{I_s \beta^3}{\rho A'} D = 0 \qquad (2.35)$$

and Eq. (2.32) $\Rightarrow$

$$\left[\frac{I_r \beta^3}{\rho A'} \sin\beta\ell - \cos\beta\ell\right] A - \left[\frac{I_r \beta^3}{\rho A'} \cos\beta\ell + \sin\beta\ell\right] B$$

$$+ \left[\cosh\beta\ell - \frac{I_r \beta^3}{\rho A'} \sinh\beta\ell\right] C + \left[\sinh\beta\ell - \frac{I_r \beta^3}{\rho A'} \cosh\beta\ell\right] = 0 \qquad (2.36)$$

Equations (2.33) - (2.36) can be recast in the matrix format as

$$\left[M(\beta)\right] \begin{bmatrix} A \\ B \\ C \\ D \end{bmatrix} = \begin{bmatrix} 0 \\ 0 \\ 0 \\ 0 \end{bmatrix} \qquad (2.37)$$

For non-trivial solution of $\phi(x)$ (Eq. 2.23) the determinant of $M(\beta)$ must be zero. A computer program was written, and the values of $\beta$, solutions of the nonlinear equation $\det [M(\beta)] = 0$, obtained.

These values of $\beta$ were substituted into

$$\omega = \beta^2 \sqrt{\frac{EI}{\rho A'}}$$

to derive the frequencies of the inplane and out-of-plane lateral vibrational modes. The results are given in Tables (2.2) and (2.3).

Table 2.2 Values of $\beta$ and Natural Frequencies ($H_z$) for the first 9 In-plane (Pitch) Bending Modes

| $\beta$ | $\omega(H_z)$ |
|---|---|
| 0.0097 | 0.3065 |
| 0.0310 | 3.1308 |
| 0.0549 | 9.81922 |
| 0.0789 | 20.2809 |
| 0.1030 | 34.562 |
| 0.1271 | 52.6288 |
| 0.1512 | 74.4794 |
| 0.1754 | 100.229 |
| 0.1995 | 129.664 |

Table 2.3 Values of β and Natural Frequencies ($H_z$) for the First 9 Out-Plane (Roll) Bending Modes

| β | $\omega(H_z)$ |
|---|---|
| 0.0103 | 0.3456 |
| 0.0310 | 3.1308 |
| 0.0549 | 9.81922 |
| 0.0789 | 20.2809 |
| 0.1030 | 34.562 |
| 0.1271 | 52.6288 |
| 0.1512 | 74.4794 |
| 0.1754 | 100.229 |
| 0.1995 | 129.664 |

II. D. Derivation of the Frequencies of the Torsional Vibration, SCOLE Configuration.

Assuming the mast to be a circular shaft, the torque at any point on the shaft is given by

$$T = GI \frac{\partial y(x,t)}{\partial x}$$

where G is the modulus of rigidity and I the polar moment of inertia of the cross sectional area of the beam. This torque is opposed by the inertial torque $I\rho \frac{\partial^2 (y(x,t))}{\partial t^2}$

where $\rho$ is the density of the beam. For equilibrium,

$$GI \frac{\partial y(x,t)}{\partial x} - I\rho \frac{\partial^2 y(x,t)}{\partial t^2} = 0 \qquad (2.38)$$

Assuming the separability of the variables, Equation (2.38) is solved to yield, solutions of the form

$$y(x,t) = f(t)\,\phi(x)$$

where

$$\left.\begin{aligned} f(t) &= \alpha \cos(\omega t) + \beta \sin(\omega t) \\ \phi(x) &= A \sin \omega\sqrt{\rho/G}\; x + B \cos \omega\sqrt{\rho/G}\; x \end{aligned}\right\} (2.39)$$

## Boundary Conditions

Writing that the torque, T, at either and of the beam equals the moment of inertia times the angular acceleration of the interface point yields:

$$GI \frac{\partial y(x,t)}{\partial x} = I_i \frac{\partial^2 y(x,t)}{\partial t^2} \quad (2.40)$$

Equation (2.40) along with the equilibrium of the shaft gives:

for the Shuttle end: x = 0

$$GI \left.\frac{\partial y(x,t)}{\partial x}\right|_{x=0} = - I_s \omega^2 \left. y(x,t)\right|_{x=0} \quad (2.41)$$

for the reflector end: x = ℓ = 130

$$- GI \left.\frac{\partial y(x,t)}{\partial x}\right|_{x=130} = - I_r \omega^2 \left. y(x,t)\right|_{x=130} \quad (2.42)$$

After substitution of equation (2.39) into equations (2.41) and (2.42), one arrives at:

Eq. (2.41) $\Rightarrow$ $$A\, GI \sqrt{\rho/G} + B\, I_s\, \omega = 0 \quad (2.43)$$

Eq. (2.42) $\Rightarrow$

$$\left[ GI \sqrt{\rho/G} \cos \omega\ell \sqrt{\rho/G} - I_r \omega \sin \omega\ell \sqrt{\rho/G} \right] A$$

$$- \left[ GI \sqrt{\rho/G} \sin \omega\ell \sqrt{\rho/G} + I_r \omega \cos \omega\ell \sqrt{\rho/G} \right] B = 0 \quad (2.44)$$

Equations (2.43) and (2.44) can be recast in matrix format

as $$\begin{bmatrix} P(\omega) \end{bmatrix} \begin{bmatrix} A \\ B \end{bmatrix} = \begin{bmatrix} 0 \\ 0 \end{bmatrix} \quad (2.45)$$

For non-trivial solution of equation (2.39) one must insure that the determinant $[P(\omega)]$ is equal to zero.

The values of $\omega$ for which det $[P(\omega)] = 0$ correspond to the frequencies of the torsional vibration. A computer program was written to solve this determinental equation and the frequencies for the torsional modes are listed in Table 2.4.

Table 2.4 Values of Natural Frequencies ($H_z$) for the First 9 Torsional Vibration Modes

| $\omega(H_z)$ |
|---|
| 0.0305 |
| 39.99 |
| 79.98 |
| 119.97 |
| 157.97 |
| 199.96 |
| 239.55 |
| 279.94 |
| 319.939 |

## II.E Preliminary Calculation of the SCOLE Appendage Frequencies based on Finite Element Techniques

For this application both the reflector and the mast are assumed to be a single flexible body. This body is considered to be comprised of two types of elements: (1) beam elements; and (2) triangular plate elements. The actual finite element model (FEM) is described as follows:

Mass distribution

| | |
|---|---|
| Space Shuttle | 6,366.46 slug |
| Mast | 12.42 slug |
| Reflector | 12.42 slug |

The masses of the reflector and the mast being so small (.39%) as compared with the mass of the orbiter, which in this analysis is assumed rigid, the system could be modelled as a cantilever beam (mast) with a mass with inertia (reflector) at its end. Also, the reflector in this section is going to be assumed flat with a constant thickness small as compared with its characteristic dimensions.

The dynamics analysis of the STRUDL software package, which uses a physical analysis to solve the equations of dynamic equilibrium, is used to generate the eigenvalues, the frequencies, and the periods of the system.

System Geometry (Model)

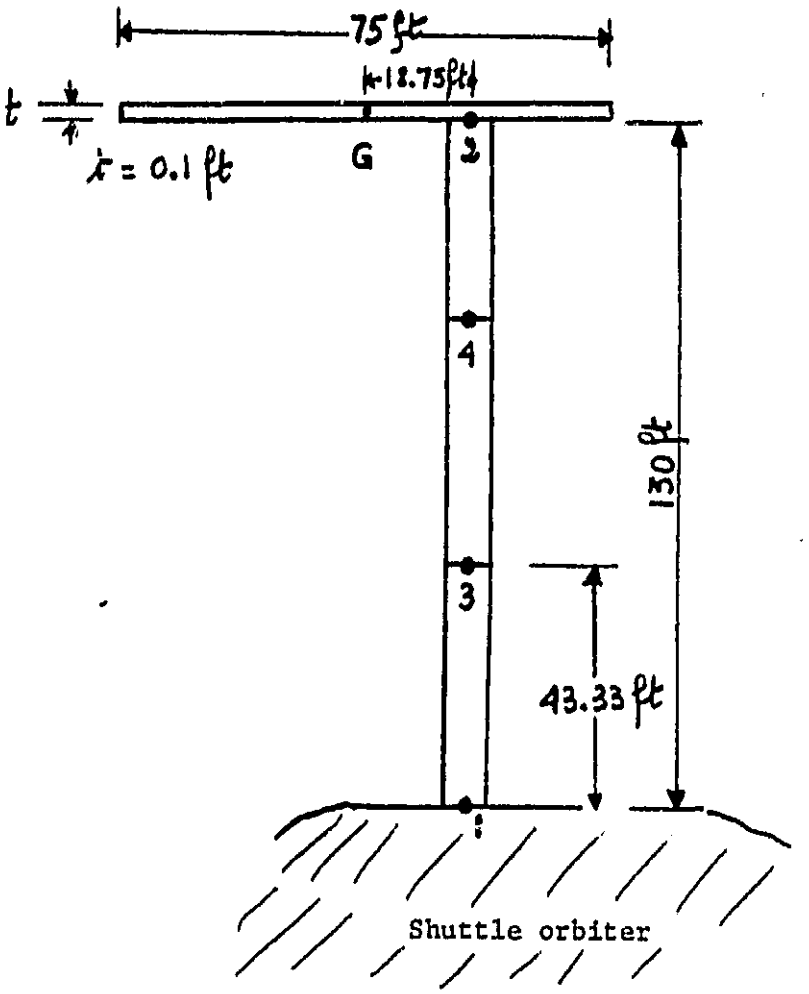


The beam (mast) will be divided into 3 beam elements (each of 43.33ft length) having a mass of 4.14 slug to be lumped at the ends of the elements.

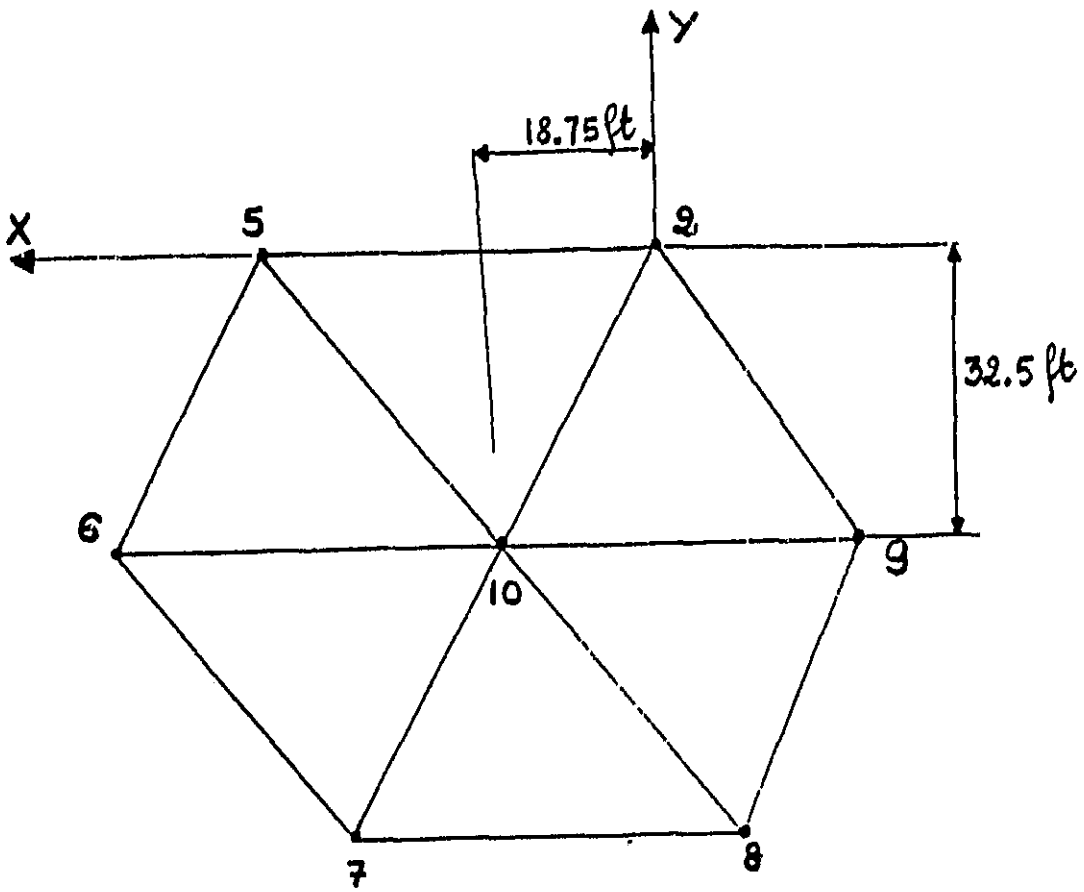


Coordinates of nodes for the System

| Node No. | X | Y | Z | in ft. |
|---|---|---|---|---|
| 1. | 0.0 | 0.0 | 0.0 | |
| 2. | 0.0 | 0.0 | -130.0 | |
| 3. | 0.0 | 0.0 | - 43.33 | |
| 4. | 0.0 | 0.0 | - 86.66 | |
| 5. | 37.50 | 0.0 | -130.00 | |
| 6. | 56.25 | -32.50 | -130.00 | |
| 7. | 37.50 | -65.00 | -130.00 | |
| 8. | 00.00 | -65.00 | -130.00 | |
| 9. | -18.75 | -32.50 | -130.00 | |
| 10. | 18.75 | -32.50 | -130.00 | |

## Results - Conclusions

The following results have been obtained (Table 2.5). They show that the system is less stiff in this model as compared with previously developed NASA[8] and Howard University continuum models and also that recently described by the Harris Corporation.[9]

Table 2.5 - Modal Frequencies ($H_z$) Obtained by Implementing a FEM of the Preliminary Model of SCOLE (Poisson's ratio = 0.3 assumed)

| |
|---|
| 0.157 |
| 0.275 |
| 0.782 |
| 1.083 |
| 1.232 |
| 1.386 |
| 80.09 |
| 107.24 |
| 107.24 |
| 265.99 |
| 421.50 |

II.F Linearization of the Equation of Motion-Floquet Analysis

Let $\tau$ the dimensionaless time be equal to $\omega_c t$; $\frac{d}{dt} = \omega_c \frac{d}{d\tau}$ ;

$\frac{d^2}{d\tau^2} = \omega_c^2 \frac{d^2}{d\tau^2}$

Dividing each term of Eq. (2.16) by $M_m \ell$ yields

$$- \ddot{\theta} \left\{ I_{zs}/M_m \ell + \ell/3 + I_{zr}/M_m \ell + \frac{Mr}{Mm} \frac{X}{\ell} x + \frac{Mr}{Mm} R_2 \right\}$$

$$+ \left\{ \left( \frac{R}{\ell} - \frac{Mr}{Mm} \frac{R}{\ell} \right) \omega_c \psi(\ell) - \omega_c \frac{R}{\beta \ell^2} \psi_1(\ell) \right\} \left( \dot{\theta} \cos(\omega t + \phi) - \theta \omega \sin(\omega t + \phi) \right)$$

$$- \frac{Mr}{Mm} \frac{X}{\ell} R \omega_c \dot{\theta} \cos(\omega t + \phi) + \omega^2 \cos(\omega t + \phi) \left\{ \left( I_{zr}/M_m \ell^2 + \frac{Mr}{Mm} + \frac{Mr}{Mm} \frac{X^2}{\ell^2} \right) \psi(\ell) \right.$$

$$\left. + \frac{1}{\beta \ell} \psi_2(\ell) + \frac{1}{\beta^2 \ell^2} \psi_3(\ell) \right\} - \omega \sin(\omega t + \phi) \cos(\omega t + \phi) \left[ \psi^2(\ell) \right] \left\{ \frac{3}{2} \frac{R}{\ell^2} \omega_c \right.$$

$$\left. - \frac{Mr}{Mm} \frac{R}{\ell^2} \omega_c \right\} - \omega \sin(\omega t + \phi) \psi(\ell) \frac{Mr}{Mm} \frac{X}{\ell} \frac{R}{\ell} \omega_c = 0 \qquad (2.46)$$

Let now $C_1 = \left\{ I_{zs}/M_m \ell + \ell/3 + I_{zr}/M_m \ell + \mu \lambda X + \mu R_2 \right\}$

where $\mu = \frac{M_r}{M_m}$ ; $\lambda = \frac{X}{\ell}$

$$C_2 = \left( \frac{R}{\ell} - \mu \frac{R}{\ell} \right) \psi(\ell) - \frac{R}{\beta \ell^2} \psi_1(\ell)$$

where $\psi(\ell) = A \cos \beta\ell + B \sin \beta\ell + C \cosh \beta\ell + D \sinh \beta\ell$

$\psi_1(\ell) = A \sin \beta\ell \mp B \cos \beta\ell + C \sinh \beta\ell + D \cosh \beta\ell + B - D$

$$C_3 = \left( I_{zr}/M_m \ell^2 + \mu + \mu \lambda^2 \right) \psi(\ell) + \psi_2(\ell)/\beta\ell + \psi_3(\ell)/\beta^2 \ell^2$$

where $\psi_2(\ell) = A \sin \beta\ell - B \cos \beta\ell + C \sinh \beta\ell + D \cosh \beta\ell$

$\psi_3(\ell) = A \cos \beta\ell + B \sin \beta\ell - C \cosh \beta\ell - D \sinh \beta\ell - A + C$

$$C_4 = (\psi(\ell))^2 \left\{ \frac{3}{2} \frac{R}{\ell^2} - \mu \frac{R}{\ell^2} \right\}$$

$$C_5 = \mu \lambda R$$

and $C_6 = \psi(\ell)\, \mu \lambda \frac{R}{\ell}$

Eq. (2.46) can be written as

$$- C_1 \ddot{\theta} + \omega_c C_2 \frac{d}{dt}(\theta \cos(\omega t + \phi)) - \omega_c C_5 \dot{\theta} + \omega^2 C_3 \cos(\omega t + \phi)$$
$$- \omega_c \omega C_4 \sin(\omega t + \phi) \cos(\omega t + \phi) - \omega \omega_c C_6 \sin(\omega t + \phi) - 3\omega_c^2 (I_{11} - I_{33}) \dot{\theta} = 0 \qquad (2.47)$$

Introducing the dimensionaless time $\tau = \omega_c t$ and dividing Eq. (2.47) by $\omega_c^2$ one arrives at

$$- \omega_c^2 C_1 \theta'' + \omega_c^2 C_2 \frac{d}{d\tau}(\theta \cos(\omega t + \phi)) - \omega_c^2 C_5 \frac{d}{d\tau}\theta$$
$$+ \omega^2 C_3 \cos(\omega t + \phi) - \omega_c \omega C_4 \sin(\omega t + \phi) \cos(\omega t + \phi) - \omega \omega_c C_6 \sin(\omega t + \phi) = 0 \qquad (2.48)$$

Introducing now the new parameter $\Omega = \frac{\omega}{\omega_c}$ yields

$$- C_1 \theta'' + C_2 \frac{d}{d\tau}[\theta \cos(\Omega\tau + \phi)] - C_5 \frac{d}{d\tau}\theta$$
$$+ \Omega^2 C_3 \cos(\Omega\tau + \phi) - \frac{\Omega C_4}{2} \sin[2(\Omega\tau + \phi)]$$
$$- \Omega C_6 \sin(\Omega\tau + \phi) - 3(I_{11} - I_{33})\theta' = 0 \qquad (2.49)$$

## Parametric Study of the System

Let us assume that the interface point between the reflector and the mast is at the center of mass of the reflector

$$\rightarrow X = 0 \rightarrow \lambda = 0 = C_5 = C_6$$

Under this assumption, the equation becomes

$$-\theta'' + \frac{C_2}{C_1}\frac{d}{d\tau}\left[\theta\cos(\Omega\tau+\phi)\right] + \Omega^2\frac{C_3}{C_1}\cos(\Omega\tau+\phi)$$
$$-\frac{C_4}{2C_1}\Omega\sin\left[2(\Omega\tau+\phi)\right] - \frac{3}{C_1}(I_{11}-I_{33})\theta' = 0 \qquad (2.50)$$

which yields the following first integral

$$-\theta' + \frac{C_2}{C_1}\left[\theta\cos(\Omega\tau+\phi)\right] + \Omega^2\frac{C_3}{C_1}\sin(\Omega\tau+\phi)$$
$$+\frac{C_4}{C_1}\cos\left[2(\Omega\tau+\phi)\right] - \frac{3}{C_1}(I_{11}-I_{33})\theta = K \qquad (2.51)$$

This equation can be plotted in the phase plane $(\theta', \theta)$ for different values of $\mu$ and $\Omega$.

## Floquet Analysis

The angular motion about an axis perpendicular to the orbit plane is described by:

$$\theta'' = \left[-\frac{C_5}{C_1} + \frac{C_2}{C_1}\cos\Omega\tau\right]\theta' - \left[\frac{C_2}{C_1}\Omega\sin\Omega\tau + \frac{3}{C_1}(I_{33}-I_{11})\right]\theta \qquad (2.52)$$

This equation can be recast into the following matrix format

$$\begin{bmatrix} \theta' \\ \theta'' \end{bmatrix} = \begin{bmatrix} P_{11} & P_{12} \\ P_{21} & P_{22} \end{bmatrix} \begin{bmatrix} \theta \\ \theta' \end{bmatrix} \qquad (2.53)$$

where

$$[P(\tau)] = \begin{bmatrix} -\frac{C_3}{C_1} + \frac{C_2}{C_1}\cos\Omega\tau & -\left[\frac{C_2}{C_1}\Omega\sin(\Omega\tau) + \frac{3}{C_1}(I_{11} - I_{33})\right] \\ 1 & 0 \end{bmatrix}$$

Since $P(\tau)$ is a matrix with periodic coefficients, the stability of the motion will be analyzed in what follows using the Floquet theorem.

Case 1. No gravity gradient, No offset

$$p(\tau) = \begin{bmatrix} \frac{C_2}{C_1}\cos\Omega\tau & -\frac{C_2}{C_1}\Omega\sin\Omega\tau \\ 1 & 0 \end{bmatrix}$$

$$[Z(\tau)] = [P(\tau)]\,[Z(\tau)]$$

$$\dot{Z}_{11} = p_{11}Z_{11} + p_{12}Z_{21} \qquad (1)$$

$$\dot{Z}_{12} = p_{11}Z_{12} + p_{12}Z_{22} \qquad (2)$$

$$\dot{Z}_{21} = p_{21}Z_{11} + p_{22}Z_{21} \qquad (3)$$ which becomes $\dot{Z}_{21} = Z_{11}$ since $p_{21} = 1$ and $p_{22} = 0$

$$\dot{Z}_{22} = p_{21}Z_{12} + p_{22}Z_{22} \qquad (4)$$ which becomes $\dot{Z}_{22} = Z_{12}$

from (3) $\ddot{Z}_{21} = \dot{Z}_{11}$ substituted into 1 yields

$$\dot{Z}_{21} = p_{11}\dot{Z}_{21} + p_{12}Z_{21}$$

Similarily from (4) $\ddot{Z}_{22} = \dot{Z}_{12}$ which substituted into (2) yields

$$\ddot{Z}_{22} = p_{11}\dot{Z}_{22} + p_{12}Z_{22}$$

If one notices that $p_{12} = \frac{d}{dt} p_{11}$

then $$\ddot{Z}_{21} = p_{11}\dot{Z}_{21} + \dot{p}_{11}Z_{21} = \frac{d}{dt}(p_{11}Z_{21})$$

and $$\ddot{Z}_{22} = p_{11}\dot{Z}_{22} + \dot{p}_{11}Z_{22} = \frac{d}{dt}(p_{11}Z_{22})$$

These two last equations are integrated and the following result for $Z_{21}$ and $Z_{22}$ obtained

$$\dot{Z}_{21} = p_{11}Z_{21} + K_1$$

$$\dot{Z}_{22} = p_{11}Z_{22} + K_2$$

but from (3), $\dot{Z}_{21} = Z_{11}(\tau)$ and

from (4), $\dot{Z}_{22} = Z_{12}(\tau)$

therefore, $\dot{Z}_{21}(0) = Z_{11}(0) = 1 = p_{11}(0)Z_{21}(0) + K_1$

or for $\phi = 0$ $\qquad 1 = K_1$ $\qquad$ since $Z_{21}(0) = 0$

$$\therefore K_1 = 1$$

$$\dot{Z}_{22}(0) = Z_{12}(0) = 0 = p_{11}(0)\, Z_{22}(0) + K_2$$

or for $\phi = 0$ $\qquad \frac{C_2}{C_1} = -K_2$ since $Z_{22}(0) = 1$

$$\dot{Z}_{21} = p_{11} Z_{21} + 1$$

$$\dot{Z}_{22} = p_{11} Z_{22} - \frac{C_2}{C_1}$$

Solution of the linear first order equation

$$\frac{dZ_{22}}{d\tau} - p_{11} Z_{22} = -\frac{C_2}{C_1} \tag{1}$$

The presence of $\frac{dZ_{22}}{d\tau}$ and $p_{11} Z_{22}$ in the equation suggests a product of the type $\phi(\tau) Z_{22}(\tau)$

but $$\frac{d}{d\tau}(\phi Z_{22}) = \frac{d\phi}{d\tau} Z_{22} + \phi \frac{d}{d\tau} Z_{22} \tag{2}$$

Multiplying (1) by $\phi(\tau)$ yields

$$\phi \frac{dZ_{22}}{d\tau} - \phi p_{11} Z_{22} = -\frac{C_2}{C_1} \phi \tag{3}$$

which can become

$$\frac{d}{d\tau}(\phi Z_{22}) = -\frac{C_2}{C_1} \phi \tag{4}$$

if one can find $\phi(\tau)$ (the integrating factor) such that

$$\frac{d\phi}{d\tau} = -\phi p_{11} \tag{5}$$

$$\Rightarrow \ln \phi(\tau) = \int -p_{11}\, d\tau = \int -\frac{c_2}{c_1} \cos \Omega\tau \, d\tau$$

$$\ln \phi(\tau) = -\frac{c_2}{c_1 \Omega} \sin \Omega\tau + K \quad \text{or}$$

$$\phi(\tau) = \exp\left[-\frac{c_2}{c_1 \Omega} \sin \Omega\tau + K\right]$$

from $\frac{d}{d\tau}(\phi z_{22}) = -\frac{c_2}{c_1}\phi(\tau)$ one arrives at

$$\phi z_{22} = \int -\frac{c_2}{c_1} \phi(\tau)\, d\tau$$

or $$z_{22} = \frac{1}{\phi(\tau)} \int -\frac{c_2}{c_1} \phi(\tau)\, d\tau$$

$$z_{11}(\tau) = \exp\left[\frac{c_2}{c_1 \Omega} \sin \Omega\tau + K\right] \left\{-\frac{c_2}{c_1} \int \exp\left[\frac{-c_2}{c_1 \Omega} \sin \Omega\tau + K\right] d\tau\right\}$$

According to Taylor's series development of a function

$$e^K \exp\left[-\frac{c_2}{c_1 \Omega} \sin \Omega\tau\right] = e^K \left\{1 - \frac{c_2}{c_1}\tau + \left(\frac{c_2}{c_1}\right)^2 \frac{\tau^2}{2} - \left(\left(\frac{c_2}{c_1}\right)^3 - \Omega^2 \frac{c_2}{c_1}\right)\frac{\tau^3}{6} + \cdots\right\}$$

which is integrated term by term to give

$$z_{22} = -\frac{c_2}{c_1} \exp\left[\frac{c_2}{c_1 \Omega} \sin \Omega\tau - K\right] \left\{\tau - \frac{c_2}{c_1}\frac{\tau^2}{2} + \frac{c_2^2}{6 c_1^2}\tau^3 - \left(\left(\frac{c_2}{c_1}\right)^3 - \Omega^2 \frac{c_2}{c_1}\right)\frac{\tau^4}{24} + K_1\right\}$$

since $z_{22}(0) = 1 \Rightarrow \quad K_1 = -\frac{c_1}{c_2}$

$$z_{22} = -\frac{c_2}{c_1} \exp\left\{\frac{c_2}{\Omega c_1} \sin \Omega\tau\right\} \left[-\frac{c_1}{c_2} + \tau - \frac{c_2}{c_1}\frac{\tau^2}{2} + \frac{c_2^2}{6 c_1^2}\tau^3 + \cdots\right]$$

Solution of $\dot{z}_{21} = p_{11} z_{21} + 1$ where $p_{11} = \frac{c_2}{c_1} \cos \Omega\tau$

$$\Rightarrow \frac{d}{d\tau}(\phi' z_{21}) = \frac{d}{d\tau}\phi' z_{21} + \phi' \frac{d}{d\tau} z_{21} \qquad (1)$$

$$\text{and} \quad \phi' \frac{d}{d\tau} z_{21} - \phi' p_{11} z_{21} = \phi' \qquad (2)$$

$$(1) = (2) \Rightarrow \quad \frac{d\phi'}{d\tau} = -\phi' p_{11}$$

$$\Rightarrow \ln \phi'(\tau) = -\frac{c_2}{\Omega c_1} \sin \Omega\tau + K' \quad \text{or}$$

$$\phi'(\tau) = \exp\left[-\frac{c_2}{c_1 \Omega} \sin \Omega\tau + K'\right]$$

from $$\frac{d}{d\tau}(\phi' z_{21}) = \phi' \Rightarrow \phi' z_{21} = \int \phi' d\tau$$

$$z_{21} = \frac{1}{\phi'} \int \phi' d\tau = \exp\left[\frac{c_2}{c_1 \Omega} \sin \Omega\tau - K'\right] \int \phi' d\tau$$

According to Taylor's series

$$\phi'(\tau) = \exp\left[-\frac{c_2}{\Omega c_1} \sin \Omega\tau\right] e^{K'} = e^{K'} \left\{1 - \frac{c_2}{c_1}\tau + \frac{c_2^2}{c_1^2}\frac{\tau^2}{2} + \left[-\left(\frac{c_2}{c_1}\right)^3 + \left(\frac{c_2}{c_1}\Omega^2\right)\right]\frac{\tau^3}{6}\right.$$

which is integrated term by term to yield

$$z_{21}(\tau) = \exp\left[\frac{c_2}{\Omega c_1}\sin\Omega\tau\right]\left\{\tau - \frac{c_2}{2c_1}\tau^2 + \frac{c_1^2}{c_1^2}\frac{\tau^3}{6} + \cdots + K_1'\right\}$$

$$z_{21}(0) = 0 \Rightarrow K_1' = 0$$

$$z_{11}(\tau) = \dot{z}_{21}(\tau) \Rightarrow$$

$$z_{11}(\tau) = \exp\left[\frac{c_2}{\Omega c_1}\sin\Omega\tau\right]\left[\frac{c_2}{c_1}\tau - \left(\frac{c_2}{c_1}\right)^2\frac{\tau^2}{2} + \ldots\right](\cos\Omega\tau - 1)$$

$$+ \exp\left[\frac{c_2}{c_1\Omega}\sin\Omega\tau\right]$$

It can easily be verified that $z_{11}(0) = \exp\left\{\frac{c_2}{c_1\Omega}\sin 0\right\} = 1$

and finally

$$\dot{z}_{22} = z_{12}(\tau)$$

$$\Rightarrow \quad z_{12}(\tau) = -\left(\frac{c_2}{c_1}\right)^2 \exp\left\{\frac{c_2}{\Omega c_1}\sin\Omega\tau\right\}\left[\tau - \frac{c_2}{c_1}\frac{\tau^2}{2} + \left(\frac{c_2}{c_1}\right)^2\frac{\tau^3}{6} + \cdots\right] \times$$

$$(\cos\Omega\tau - 1) + \left(\frac{c_2}{c_1}\cos\Omega\tau - \frac{c_2}{c_1}\right)\exp\left\{\frac{c_2}{\Omega c_1}\sin\Omega\tau\right\}$$

With the use of a computer program, the eigenvalues of the $[Z(\tau)]$ matrix are computed for $\tau$ = a period and their modulus compared with 1 to determine the values of the parameters for which the system is stable. The results of such parametric study are shown in the following stability diagram, Fig. 2.7. The large number of unstable points in the parametric space ($\Omega$, MU) are thought to be attributed to the absence of the gravity-gradient torque in the model. Future plans call for the extension of the Floquet analysis for the cases where a non-zero reflector attachment offset is considered and also where both a non-zero offset and the effects of gravity-gradient are included.

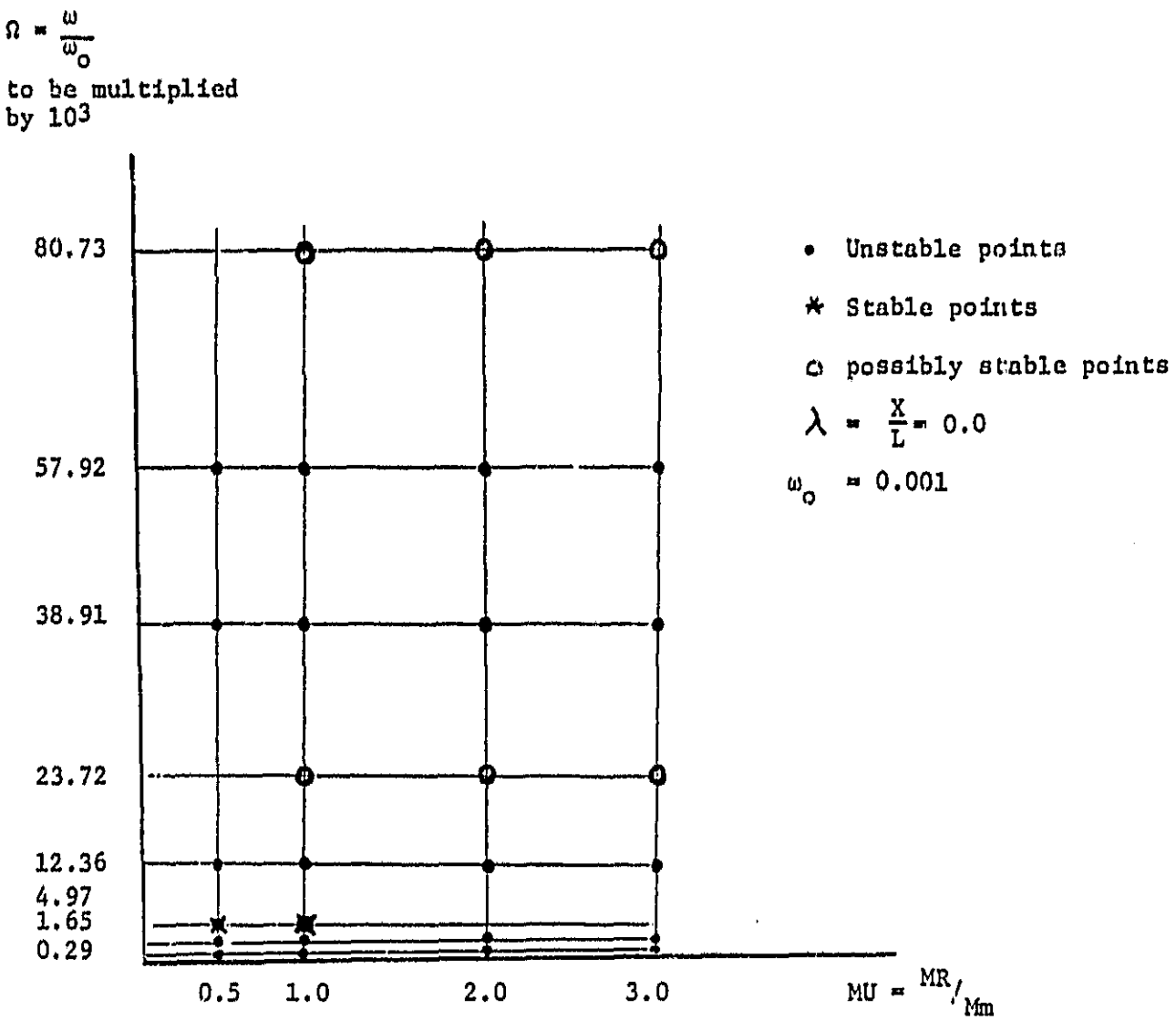


Fig. 2.7 Floquet Stability Diagram - SCOLE Configuration-No Offset No Gravity Gradient.

## References - Chapter II


1. Hale, A.L., and Lisowski, R.J., "Optimal Simultaneous Structural and Control Design of Maneuvering Flexible Spacecraft," Fourth VPI & SU/AIAA Symposium on the Dynamics and Control of Large Structures, Blacksburg, Virginia, June 6-8, 1983.

2. Bainum, P.M., Reddy, A.S.S.R., Krishna, R. and Diarra, C.M., "The Dynamics and Control of Large Flexible Space Structures-VI," Final Report, NASA Grant: NSG-1414, Suppl. 5, September 1983.

3. Bainum, P.M., Reddy, A.S.S.R., and Krishna, R., "On the Controllability and Control Law Design for an Orbiting Large Flexible Antenna System," 34th International Astronautical Congress, Budapest, Hungary, October 10-15, 1983, Paper No. IAF 83-340.

4. Montgomery, R.C., Horner, G.C., and Cole, S.R., "Experimental Research on Structural Dynamics and Control," Proceedings of the Third VPI & SU/AIAA Symposium on the Dynamics and Control of Large Flexible Spacecraft, Blacksburg, Virginia, June 15-17, 1981, pp. 365-377.

5. Taylor, L.W., Jr., and Balakrishnan, A.V., "A Laboratory Experiment Uded to Evaluate Control Laws for Flexible Spacecraft...NASA/IEEE Design Challene (SCOLE)," Fourth VPI & SU/AIAA Symposium on Dynamics and Control of Large Structures, Blacksburg, Virginia, June 6-8, 1983.

6. Likins, P.W., "Dynamics and Control of Flexible Space Vehicles," Technical Report 32-1329, Revision I, Jet Propulsion Laboratory Pasadena, California, January 15, 1970.

7. Armstrong, E.S., ORACLS, A Design System for Linear Multivariable Control, Marcel Dekker, Inc., New York and Basel, 1980.

8. Taylor, L.W., Jr., and Balakrishnan, A.V., "A Mathematical Problem and a Spacecraft Control Laboratory Experiment (SCOLE) used to Evaluate Control Laws for Flexible Spacecraft... NASA/IEEE Design Challenge, January 1984.

9. Hyland, Dave and Davis, Larry, "Application of Maximum Entropy Optimal Projection Design Synthesis to the NASA Spacecraft Control Laboratory Experiment -SCOLE," Proceedings of a Workshop Concerning the NASA-IEEE Design Challenge held at NASA Langley Research Center, Dec. 6-7, 1984 (Compiled by Larry Taylor), pp. 370-372.

## III. STABILITY OF LARGE SPACE STRUCTURES WITH DELAYED CONTROL INPUT

The dynamics of a large space structure can be represented by:

$$\dot{X}(t) = AX(t) + BU(t) \tag{3.1}$$

where

X = 2nx1 state vector

A = 2nx2n system matrix

B = 2nxm control influence matrix

U = mx1 control input vector

n = number of modes retained in the dynamic model

The matrix A for a freely vibrating large space structure has all imaginary eigenvalues and, thus, the uncontrolled system is marginally stable.

The system given in (1) can be stabilized by a state variable feedback control law of the form

$$U(t) = KX(t) \tag{3.2}$$

and

$$\dot{X}(t) = (A + BK)\, X(t) \tag{3.3}$$

such that the closed loop system matrix, (A+BK), has the required eigenvalues.

In practice, due to the high dimensionality of the state vector and the use of digital computers for evaluating control signals, there may arise a delay in the control input which can be mathematically modelled as:

$$U(t) = KX(t-\tau) \tag{3.4}$$

The consequent need to verify that the system described by

$$\dot{X}(t) = AX(t) + BKX(t-\tau) \tag{3.5}$$

is stable if the system described by equation(3.3) is stable is one of the topics of investigation carried out during the 1984-85 grant period.

The system described by equation (5) is stable [3.1] if and only if

$$-\mu(A) > ||BK|| \tag{3.6}$$

where

$$\mu(A) = \lambda_{max}(A^*+A)$$

$$||BK|| = \lambda^{\frac{1}{2}}_{max}((BK)^*(BK))$$

$A^*$, $(BK)^*$ denote the conjugate transpose of A and (BK), respectively and $\lambda_{max}(A)$ = maximum eigenvalue of matrix A.

Applying the result(3.6) to undamped large space structures (matrix A has all imaginary eigenvalues or some zero eigenvalues corresponding to the rigid body modes plus the imaginary eigenvalues corresponding to the flexible modes), we have

$$\mu(A) = 0$$

and $||BK|| > 0$

and, thus, the closed loop system becomes unstable.

In reference 3.2, the analysis of time lag systems for stability is carried out with the assumption that the original system without these delays is stable.

The large space structures pose a special problem in that the original system is marginally stable and the verification of the closed loop system stability with delayed control input has to be carried out through numerical simulation.

Two numerical simulation studies are conducted to determine the amount of time lag the system can tolerate without becoming unstable.

CASE 1:

The system under consideration is an harmonic oscillator representing an isolated vibration of a large space structure at a specific natural mode

and is given by:

$$\begin{bmatrix} \dot{x}_1 \\ \dot{x}_2 \end{bmatrix} = \begin{bmatrix} 0 & 1 \\ -\omega^2 & 0 \end{bmatrix} \begin{bmatrix} x_1 \\ x_2 \end{bmatrix} + \begin{bmatrix} 0 \\ 1 \end{bmatrix} U \tag{3.7}$$

The above system is stabilized with a control law of the form

$$U = \begin{bmatrix} 0, & -2\zeta\omega \end{bmatrix} \begin{bmatrix} x_1 \\ x_2 \end{bmatrix} \tag{3.8}$$

The numerical simulation is carried out for a control with time lag given by

$$U(t) = \begin{bmatrix} 0, & -2\zeta\omega \end{bmatrix} \begin{bmatrix} x_1(t-\tau) \\ x_2(t-\tau) \end{bmatrix} \tag{3.9}$$

with the following numerical values:

$$\begin{aligned} \omega &= 6.0 \text{ rad/sec} \\ \zeta &= 0.5 \\ x_1(0) &= 0.5 \\ x_2(0) &= 0.0 \end{aligned} \tag{3.10}$$

The time response of $x_2(t)$ is plotted for $\tau=0$, $\tau=0.085$, $\tau=0.1$ secs (DT=0.05 secs is the numerical integration step time) in Figs. 3.1, 3.2 3.3, respectively. The system became unstable for $\tau=0.1$ which is approximately one tenth of the natural frequency of oscillation of the uncontrolled system.

CASE 2:

The second system considered for numerical simulation is the dynamic model of the F-100 turbofan engine [3.3]. The uncontrolled or open loop dynamics are stable.

The system dynamics are mathematically described as:

$$\dot{X}(t) = AX(t) + BU(t) \tag{3.11}$$

The controller is of the form

$$U(t) = KX(t) \tag{3.12}$$

The matrices A,B,K and the eigenvalues of the matrices A and (A+BK) are given in Table 3.1.

The numerical simulation is carried out for the controller of the form,

$$U(t) = KX(t-\tau) \tag{3.13}$$

with the initial conditions

$$x_1(0) = x_2(0) = x_3(0) = x_4(0) = x_5(0) = 0.1$$

for $\tau$=0, $\tau$=0.001 and $\tau$=0.0099, and given in Figs 3.4, 3.5, and 3.6, respectively. The system became unstable for $\tau$=0.0099 which is a very small fraction of the period of the highest damped frequency of vibration of the uncontrolled system.

Conclusion

As the stability criteria for systems with delayed state variable feedback (as reported in the literature) are found unsuitable to apply to large space structures, which are marginally stable without control, the numerical simulation is carried out to determine the tolerable time delay without the closed loop system becoming unstable. It is observed that even very small delays can cause the closed loop system to be unstable, thus demanding the necessity of very robust controllers.

## References


3.1 Mori, T., Fukuma, N., and Kuwahara, M., "Simple Stability Criteria for Single and Composite Linear Systems with Delays," Int. J. of Control, 1981, Vol. 34, No. 6, pp. 1175-1184.

3.2 Gates, O.B., and Schy, A.A., "A Theoretical Method of Determining the Control Gearing and Time Lag Necessary for a Specified Damping of an Aircraft Equipped with a Constant-Time-Lag Autopilot," NACA TN 2307, March 1951.

3.3 Farrar, F.A., and Eidens, R.S., "Microprocessor Requirements for Implementing Modern Control Logic," IEEE Trans. on AC, Vol. AC-25, No.3, June 1980, pp. 461-468.

```
****** A MATRIX******
 -.340130E+02    -.930300E+01     .120370E+02    -.239800E+01    -.125400E+01
  .438900E+01    -.387620E+02    -.422100E+01     .284800E+02     .147290E+02
 -.475500E+01     .228700E+01    -.400000E+00    -.154600E+01    -.220000E+01
  .204600E+01     .106200E+01    -.154600E+01    -.215000E+01    -.624000E+00
  .415000E+01    -.881400E+01    -.220000E+01     .747700E+01     .109900E+01
****** B MATRIX******
  .766000E+00     .546000E+00    -.823000E+00     .170950E+02
  .560000E-01     .134100E+01     .773700E+01     .864100E+01
  .156000E+00    -.117600E+01    -.416000E+00     .203400E+01
 -.138000E+00    -.240000E-01    -.555000E+00    -.378000E+00
 -.472900E+01     .874000E+00     .161700E+01     .223000E+00
****** K MATRIX******
  .160200E+01    -.118300E+01     .222400E+01     .148000E+00     .553000E+01
  .120000E-01     .307400E+01    -.341000E+00    -.903000E+00    -.223000E+00
 -.294200E+01    -.506400E+01     .554400E+01    -.222200E+01     .814800E+01
 -.436200E+01     .749000E+00    -.652000E+00    -.920000E-01    -.811000E+00
COEFFS OF D(SI-A)
  .304472E+06     .329932E+06     .187943E+06     .107449E+05
  .188759E+03     .100000E+01
```

EIGEN VALUES OF A MATRIX

-3.48100

-2.13506±j1.12170

-33.23750±j1.40728

EIGEN VALUES OF (A+BK) MATRIX

```
 -.923823E+00    -.977062E+00
 -.923823E+00     .977062E+00
 -.288384E+02     .000000E+00
 -.588489E+02     .000000E+00
 -.992237E+02     .000000E+00
```

Table 3.1 SYSTEM MATRICES AND EIGEN VALUES

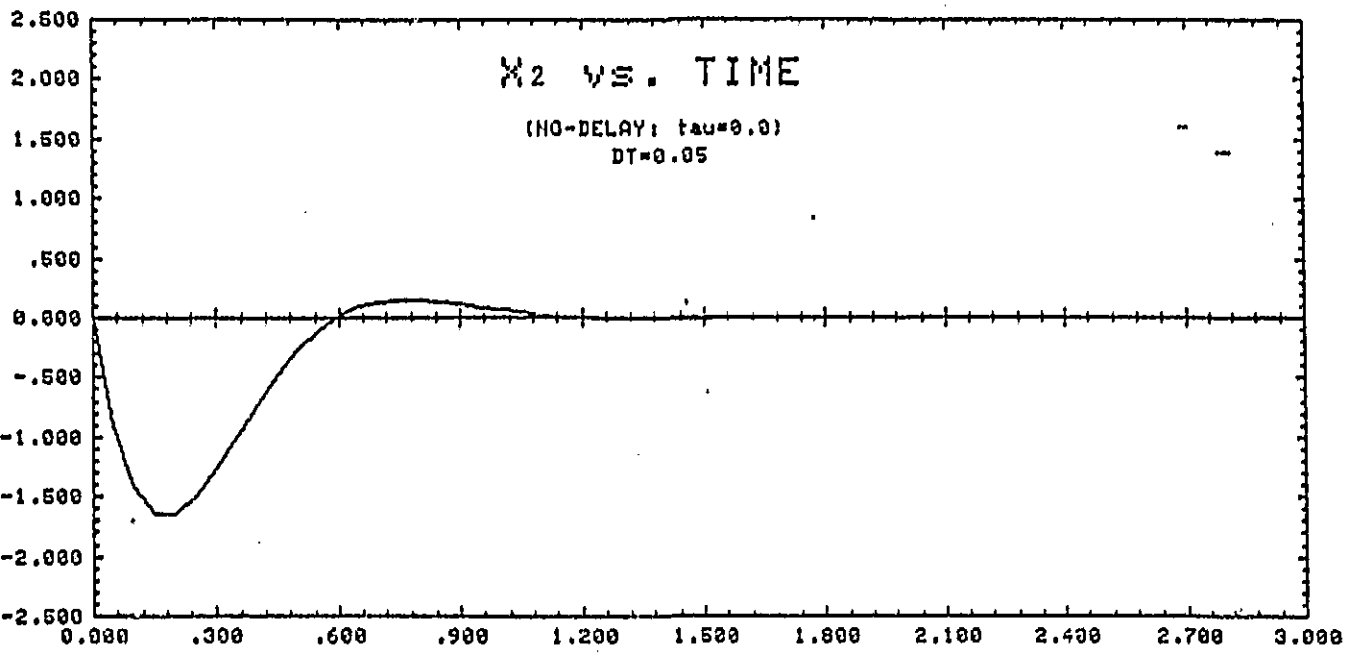


Fig. 3.1

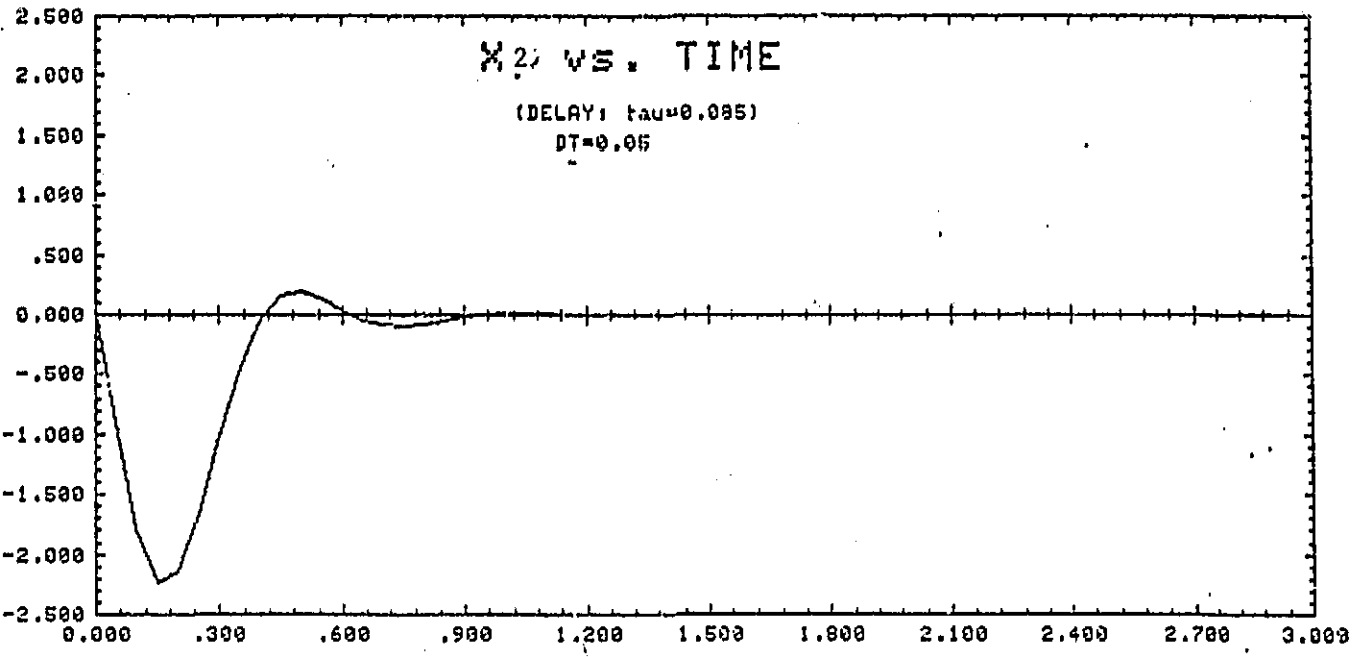


Fig. 3.2

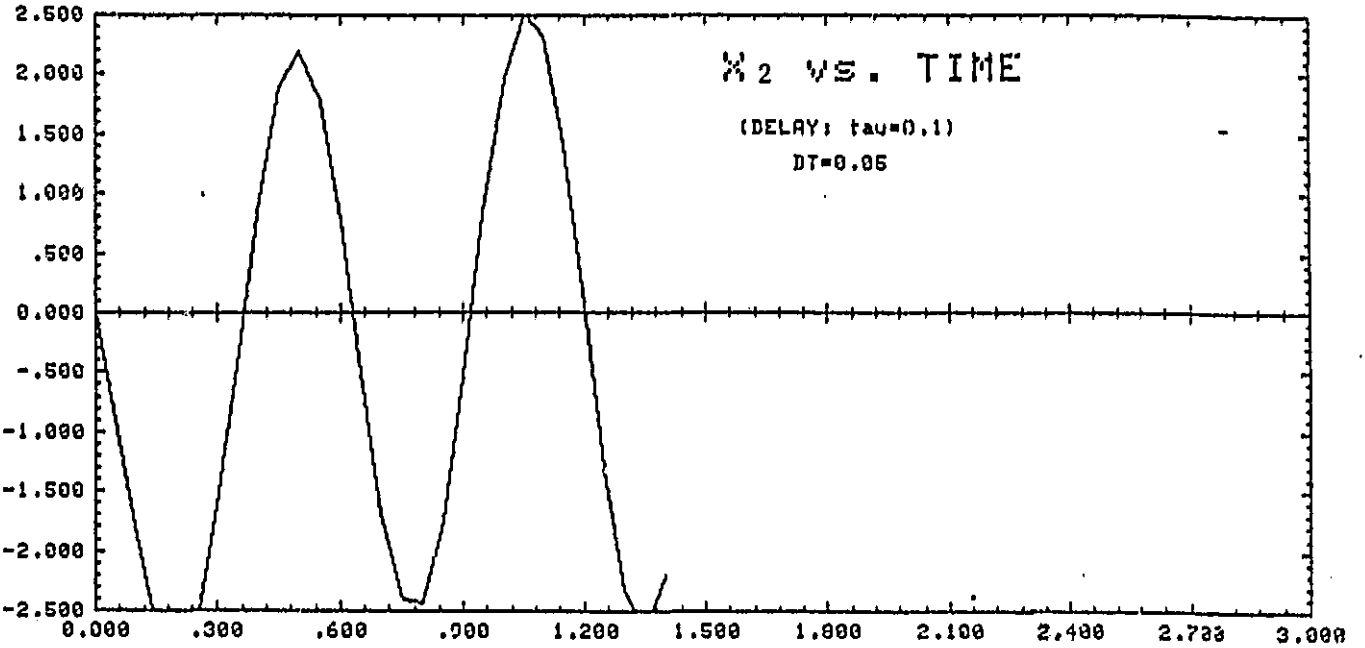


Fig. 3.3

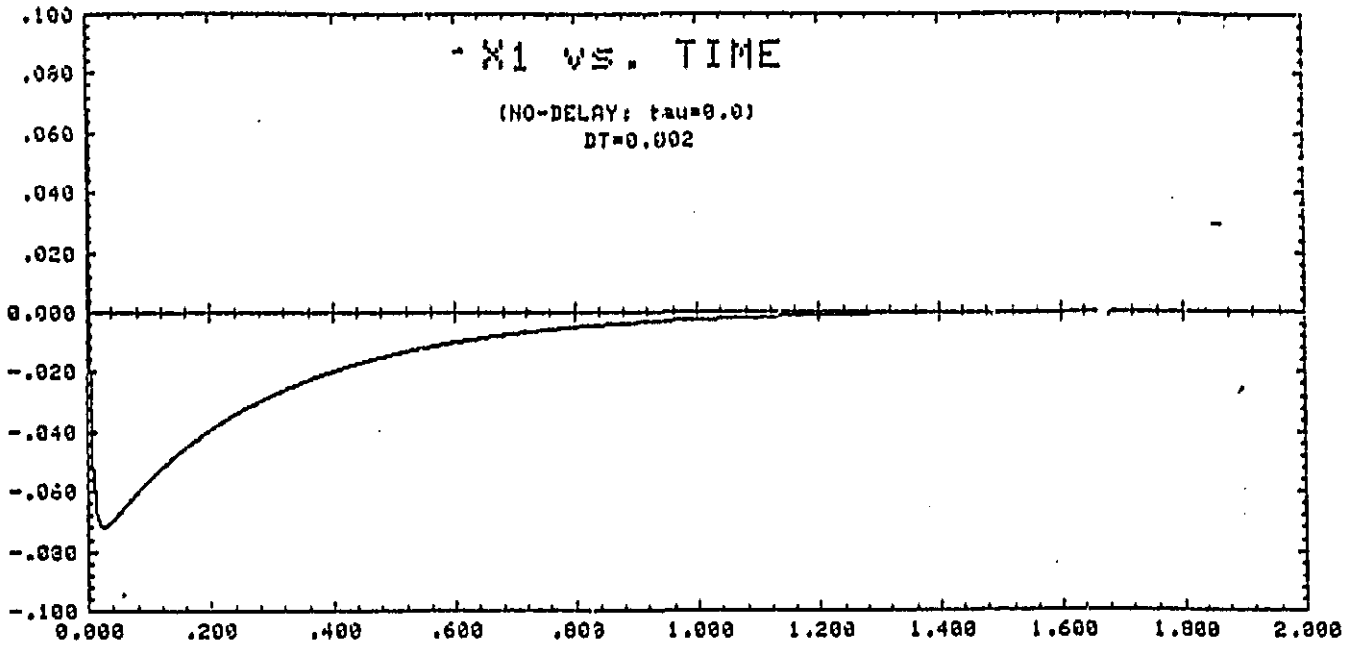
-X1 vs. TIME
(NO-DELAY; tau=0.0)
DT=0.002
.100
.080
.060
.040
.020
0.000
-.020
-.040
-.060
-.080
-.100
0.000
.200
.400
.600
.800
1.000
1.200
1.400
1.600
1.800
2.000

Fig. 3.4A

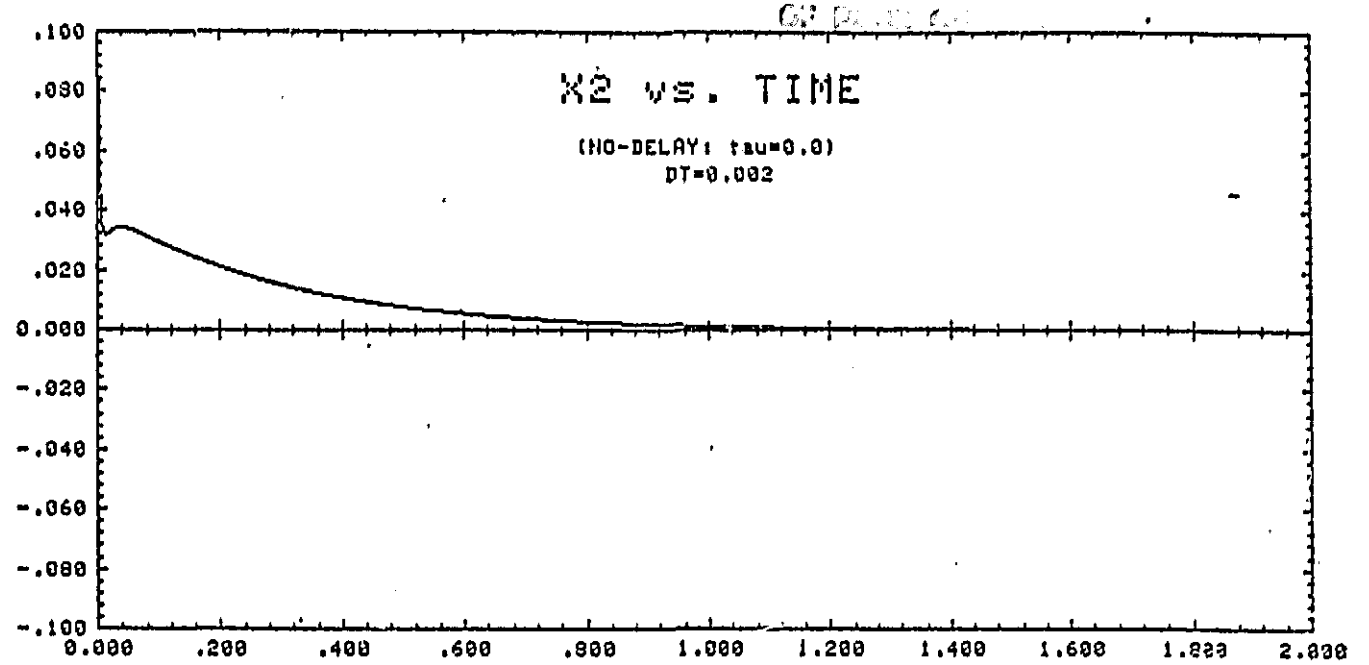
X2 vs. TIME
(NO-DELAY: tau=0.0)
DT=0.002
.100
.080
.060
.040
.020
0.000
-.020
-.040
-.060
-.080
-.100
0.000
.200
.400
.600
.800
1.000
1.200
1.400
1.600
1.800
2.000

Fig. 3.4B

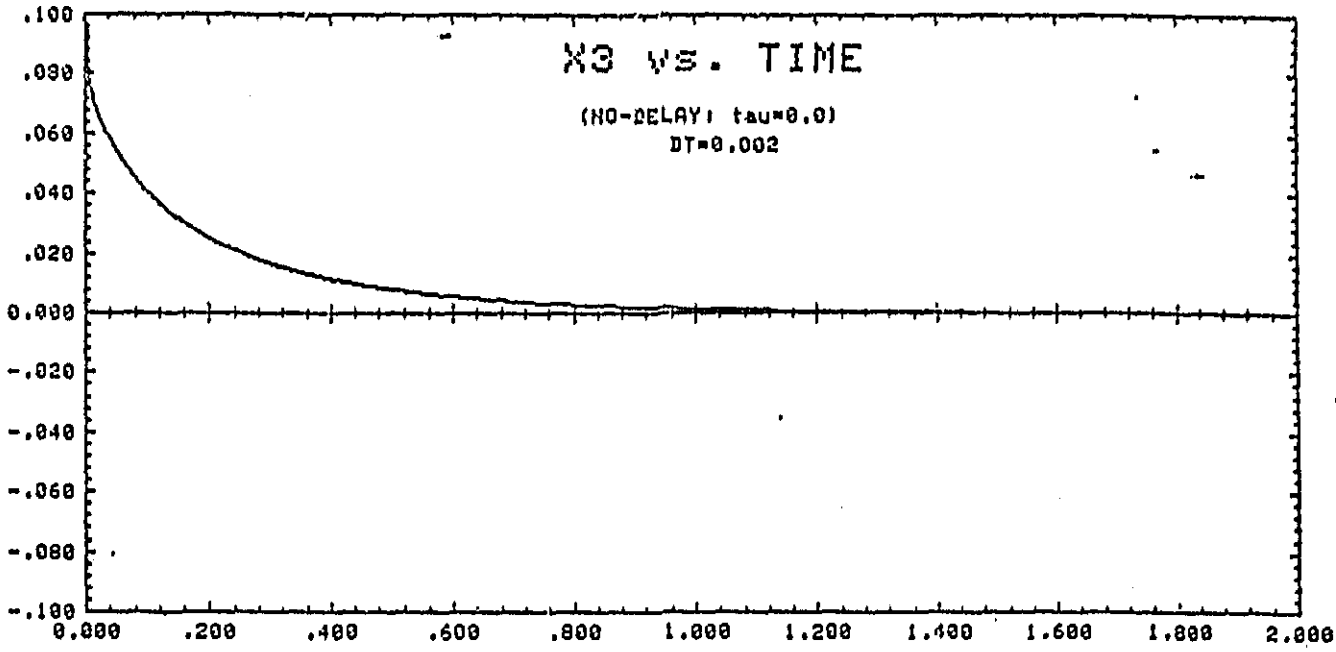
X3 vs. TIME
(NO-DELAY: tau=0.0)
DT=0.002
.100
.080
.060
.040
.020
0.000
-.020
-.040
-.060
-.080
-.100
0.000
.200
.400
.600
.800
1.000
1.200
1.400
1.600
1.800
2.000

Fig. 3.4C

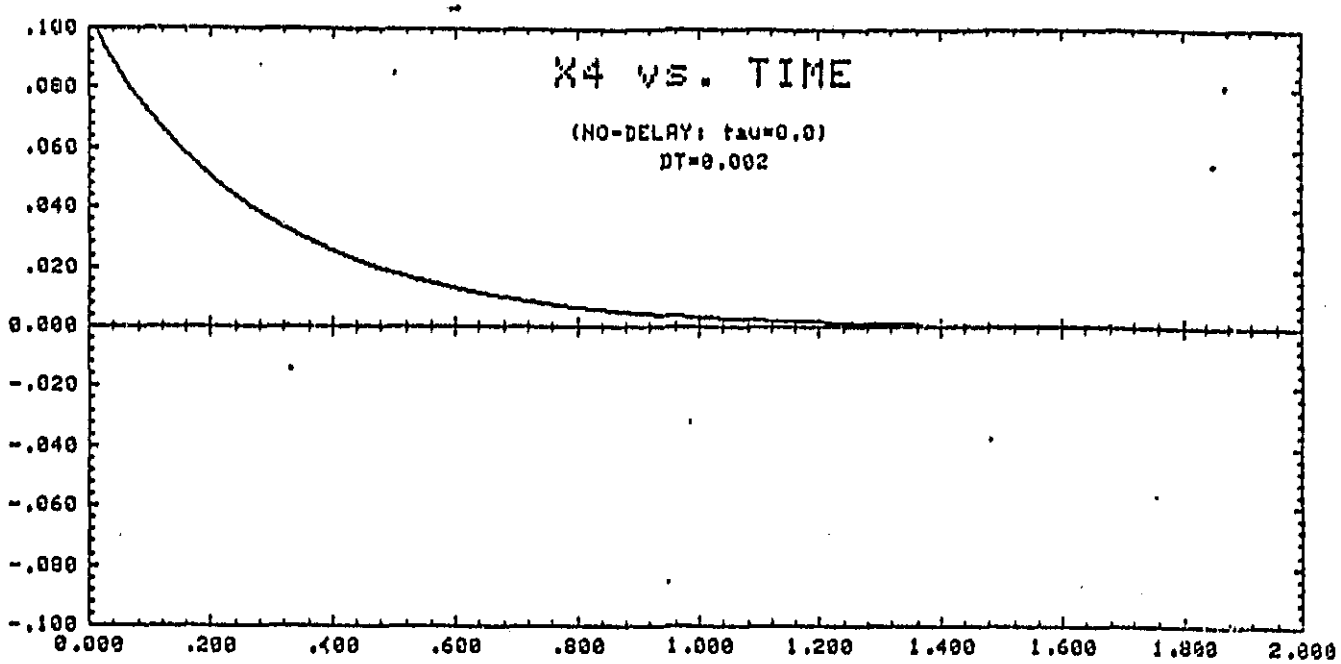
X4 vs. TIME
(NO-DELAY: tau=0.0)
DT=0.002
.100
.080
.060
.040
.020
0.000
-.020
-.040
-.060
-.080
-.100
0.000
.200
.400
.600
.800
1.000
1.200
1.400
1.600
1.800
2.000

Fig. 3.4D

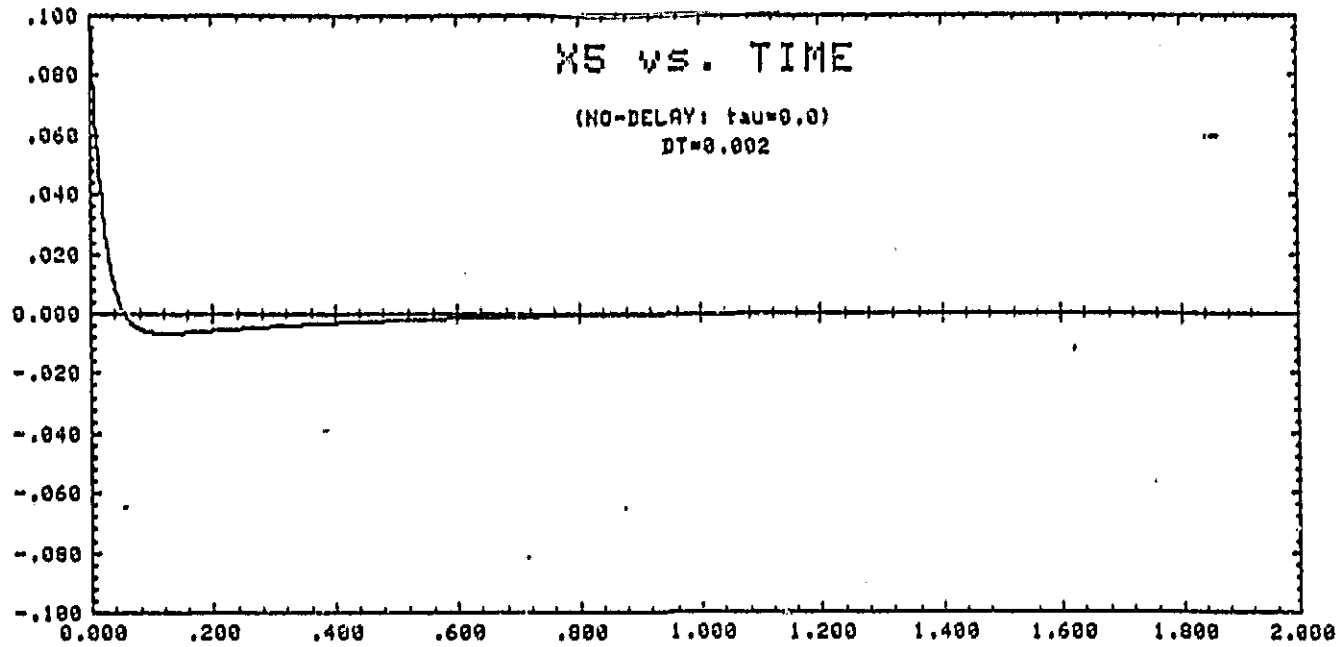


Fig. 3.4E

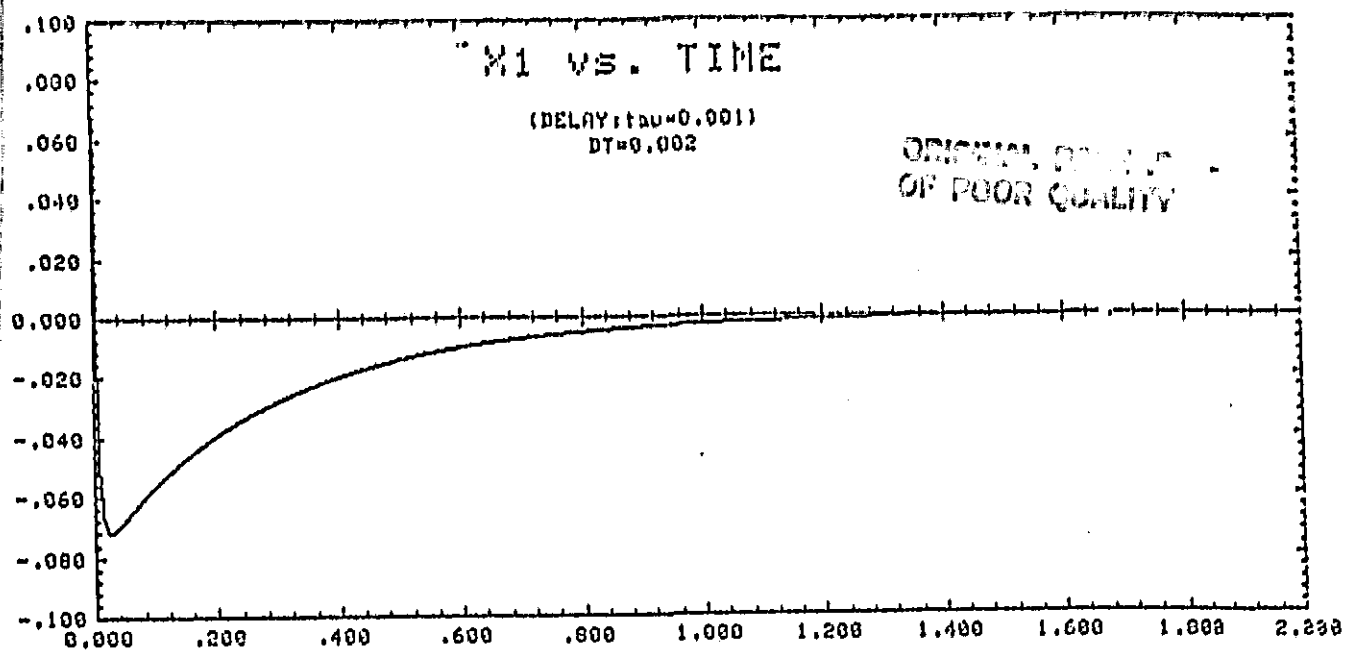




Fig. 3.5A

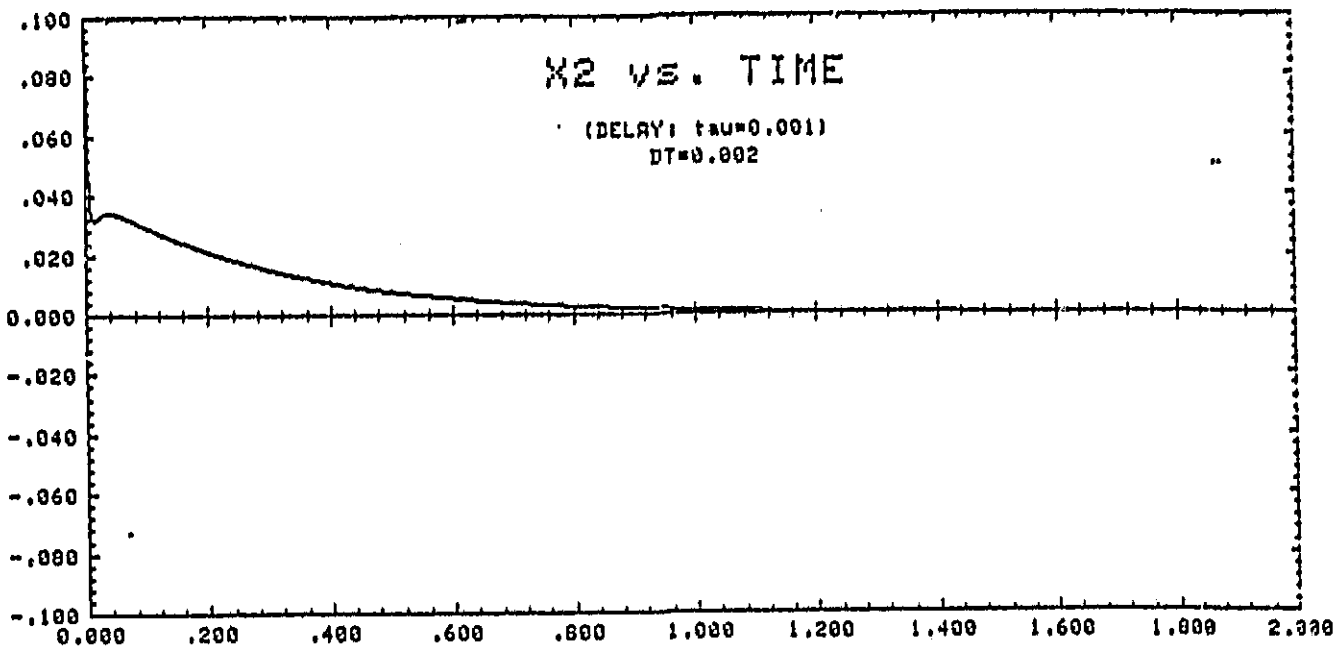
X2 vs. TIME
(DELAY: tau=0.001)
DT=0.002
.100
.080
.060
.040
.020
0.000
-.020
-.040
-.060
-.080
-.100
0.000
.200
.400
.600
.800
1.000
1.200
1.400
1.600
1.800
2.000

Fig. 3.5B

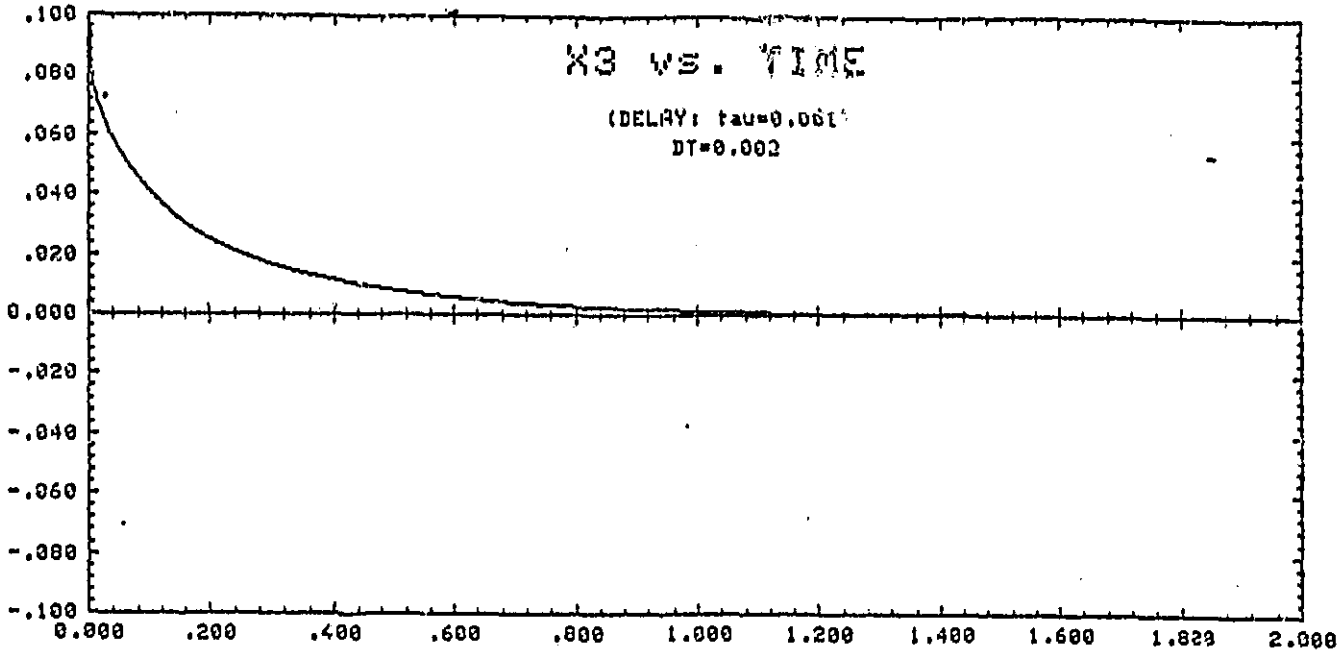
X3 vs. TIME
(DELAY: tau=0.061
DT=0.002
.100
.080
.060
.040
.020
0.000
-.020
-.040
-.060
-.080
-.100
0.000
.200
.400
.600
.800
1.000
1.200
1.400
1.600
1.829
2.000

Fig. 3.5C

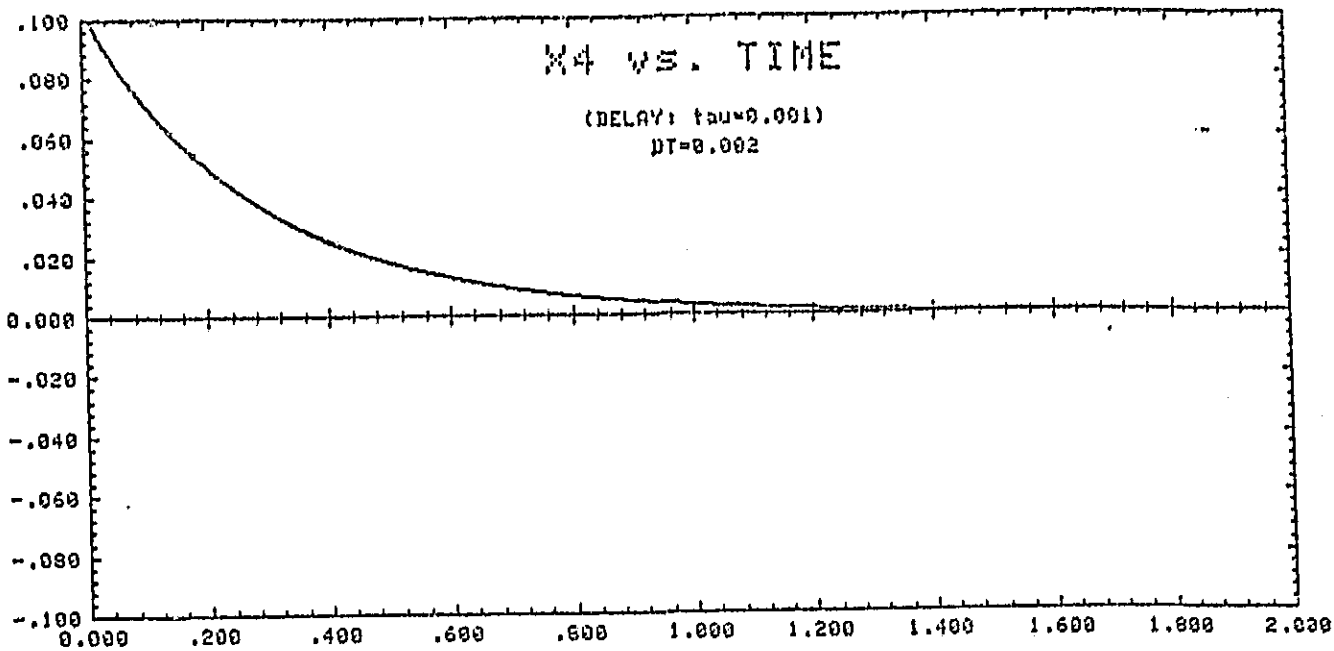


Fig. 3.5D

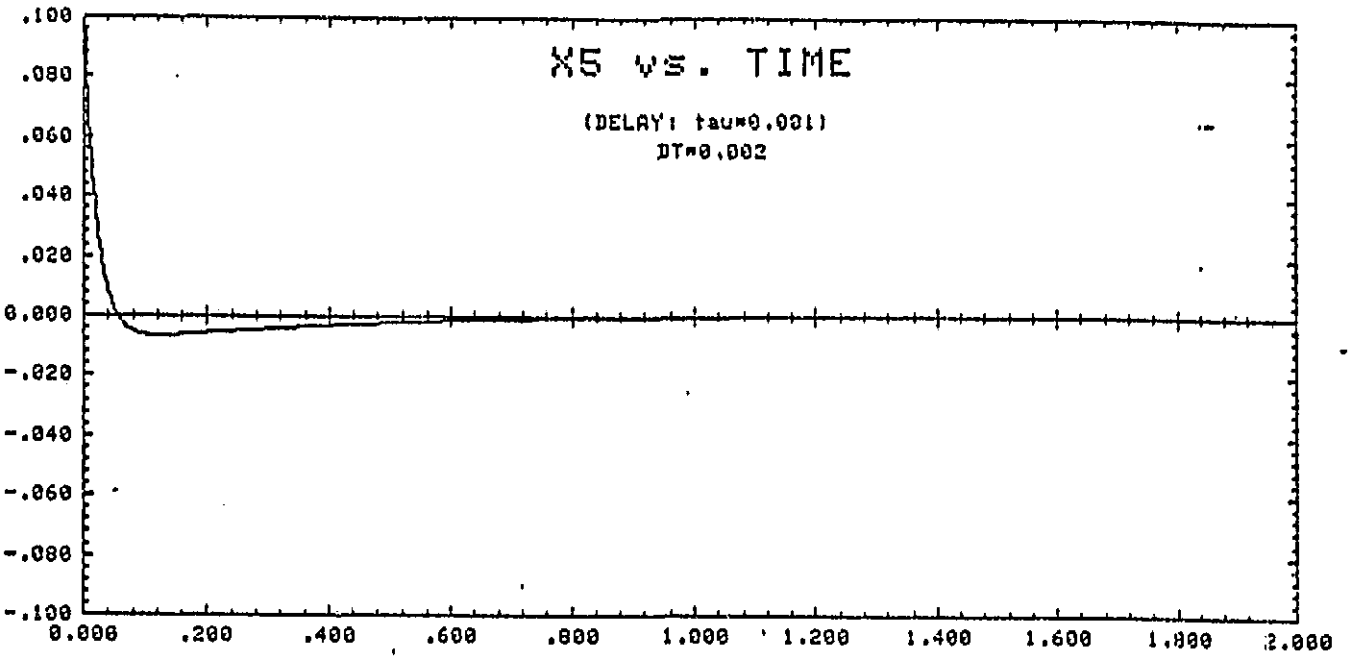
X5 vs. TIME
(DELAY: tau=0.001)
DT=0.002
.100
.080
.060
.040
.020
0.000
-.020
-.040
-.060
-.080
-.100
0.000
.200
.400
.600
.800
1.000
1.200
1.400
1.600
1.800
2.000

Fig. 3.5E

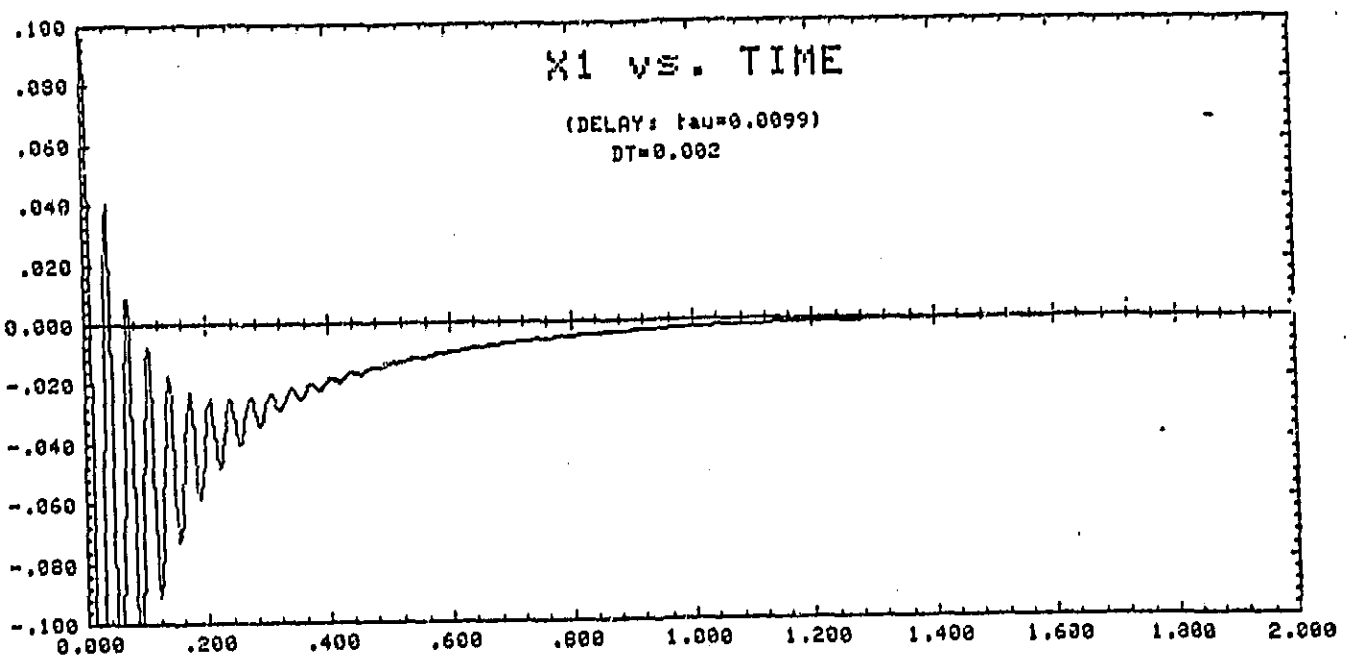
X1 vs. TIME
(DELAY: tau=0.0099)
DT=0.002
.100
.080
.060
.040
.020
0.000
-.020
-.040
-.060
-.080
-.100
0.000
.200
.400
.600
.800
1.000
1.200
1.400
1.600
1.800
2.000

Fig. 3.6A

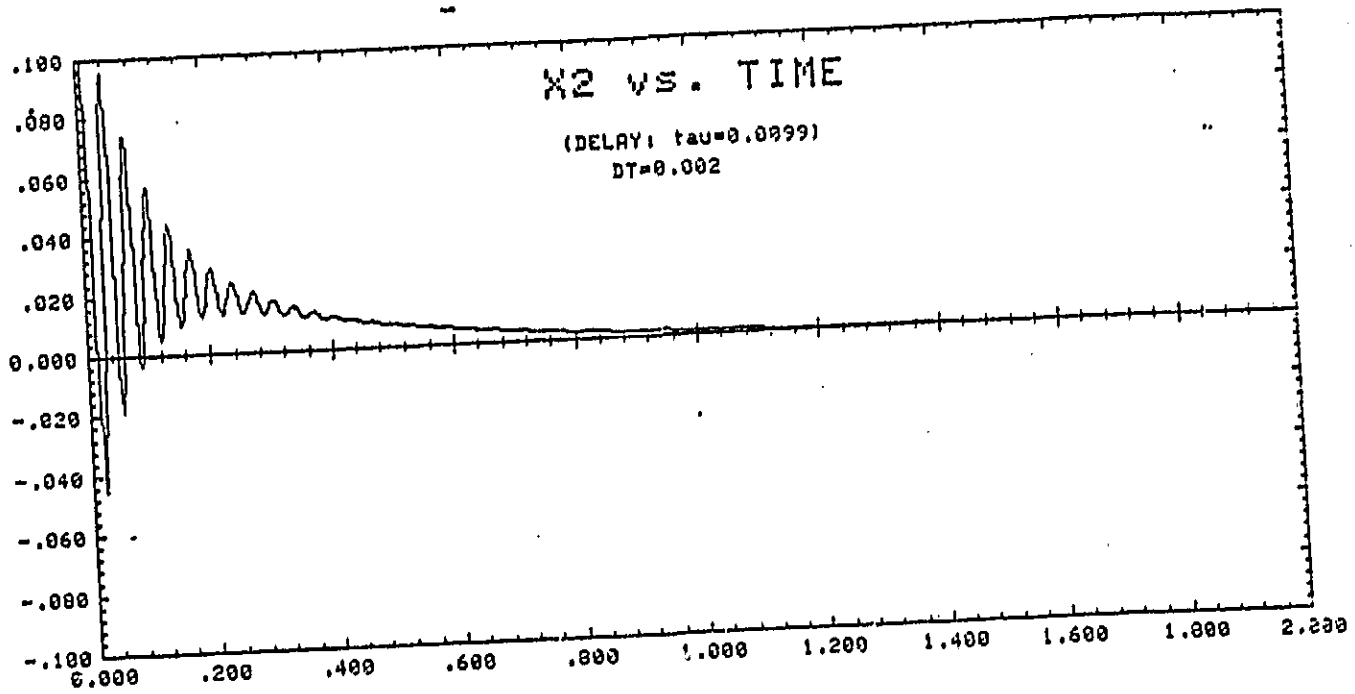


Fig. 3.6B

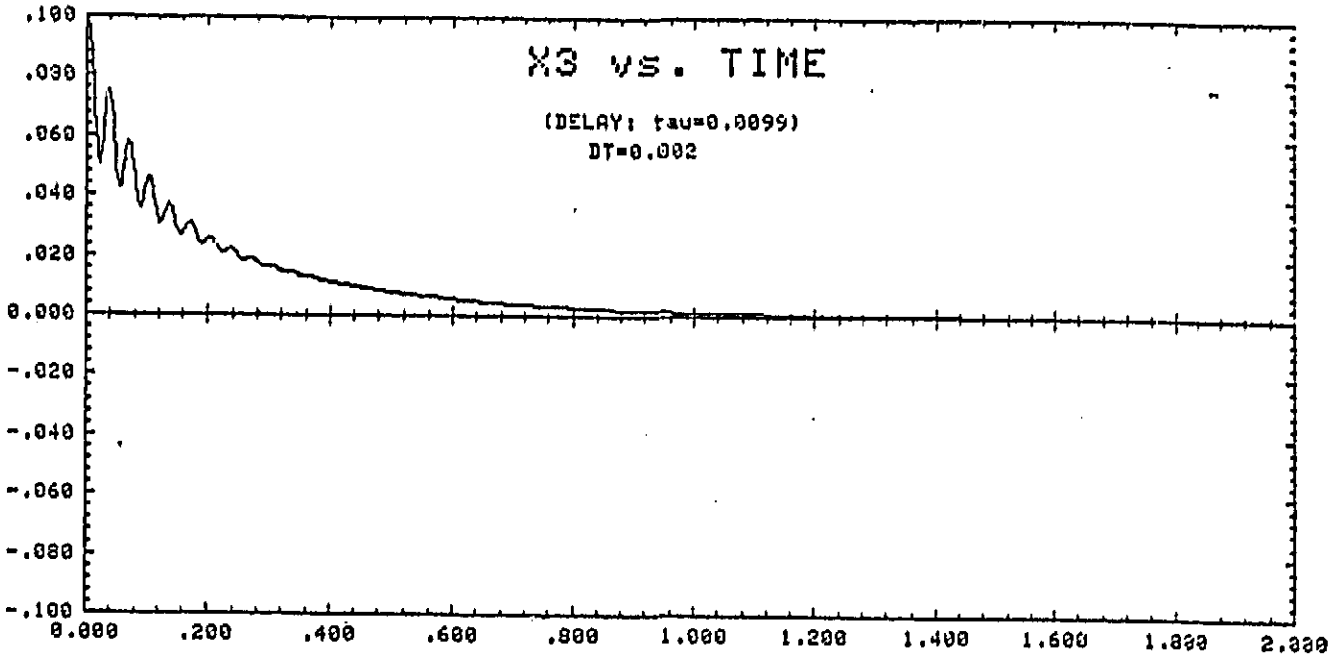
X3 vs. TIME
(DELAY: tau=0.0099)
DT=0.002
.100
.080
.060
.040
.020
0.000
-.020
-.040
-.060
-.080
-.100
0.000
.200
.400
.600
.800
1.000
1.200
1.400
1.600
1.800
2.000

Fig. 3.6C

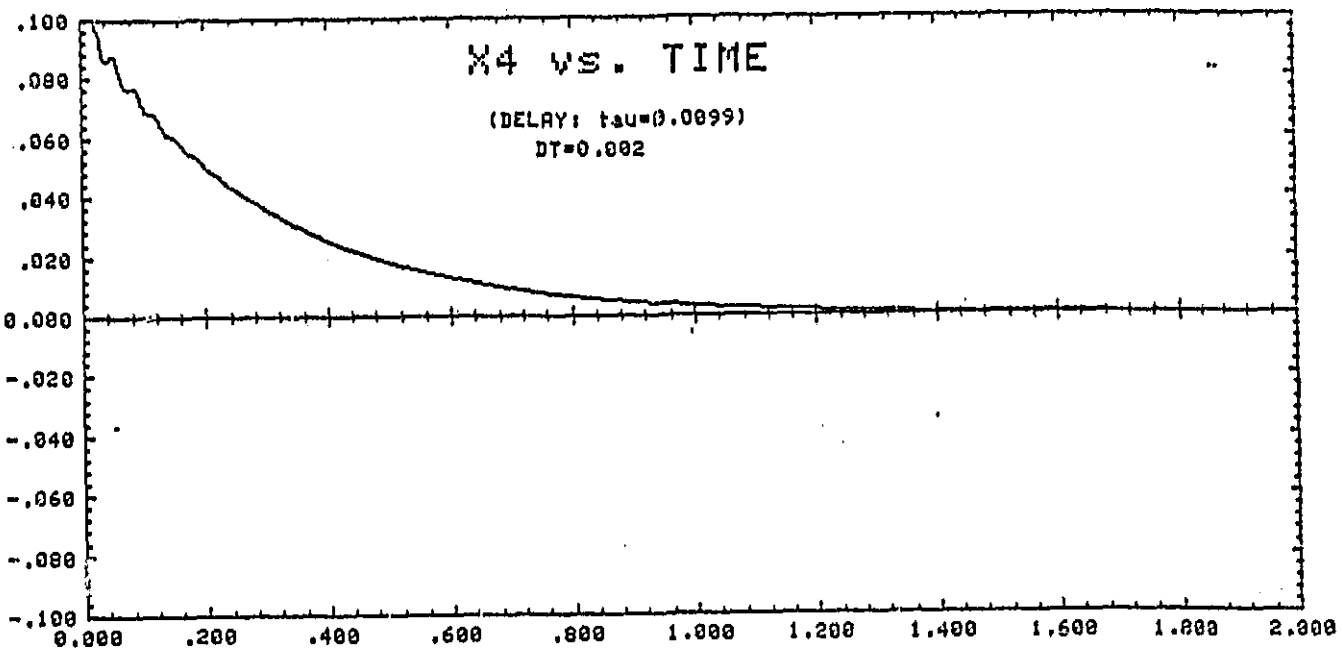
X4 vs. TIME
(DELAY: tau=0.0099)
DT=0.002
.100
.080
.060
.040
.020
0.000
-.020
-.040
-.060
-.080
-.100
0.000
.200
.400
.600
.800
1.000
1.200
1.400
1.600
1.800
2.000

Fig. 3.6D

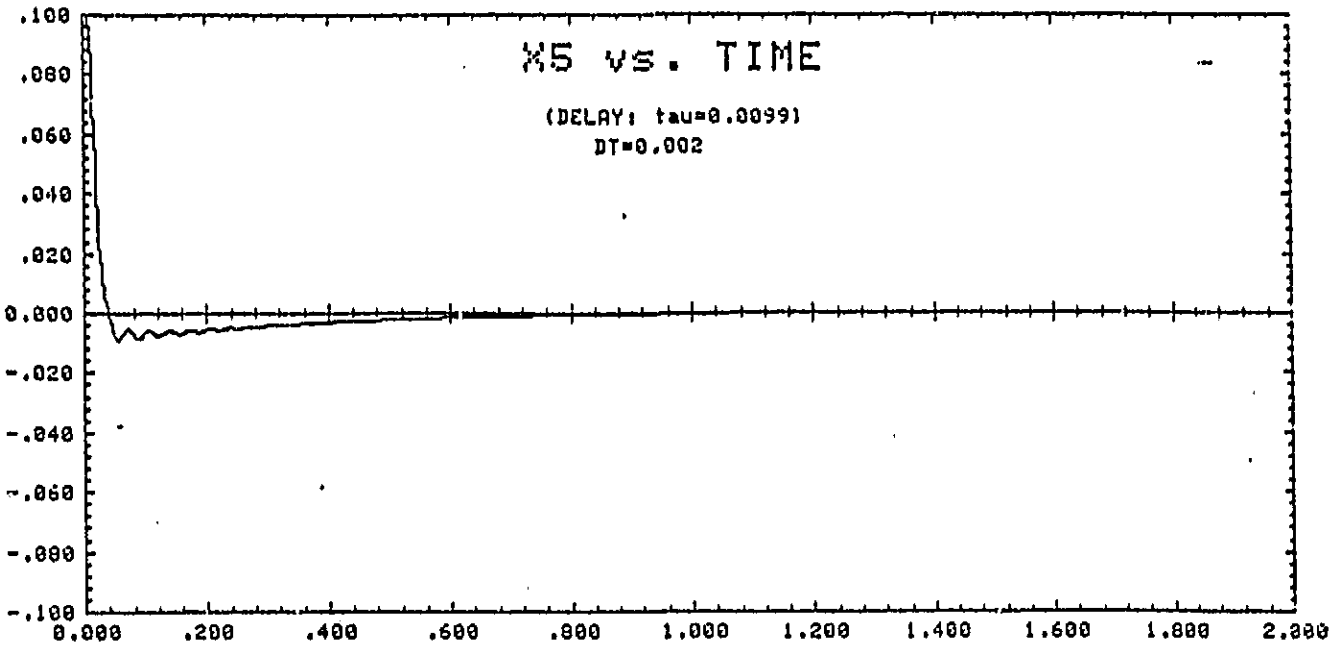
X5 vs. TIME
(DELAY: tau=0.0099)
DT=0.002
.100
.080
.060
.040
.020
0.000
-.020
-.040
-.060
-.080
-.100
0.000
.200
.400
.600
.800
1.000
1.200
1.400
1.600
1.800
2.000

Fig. 3.6E

# IV. EVALUATION OF PERFORMANCE CHARACTERISTICS FOR A SPACE ANTENNA SYSTEM SUBJECTED TO STOCHASTIC DISTURBANCES


## Abstract

The problem of controlling a stochastic linear system representing the Hoop/Column dynamics by minimization of a quadratic Gaussian performance index, appropriately weighted in both the state variables as well as the control inputs, is considered. An optimal control law for the finite element model of the Hoop/Column structural system without damping is realized by combination of the Kalman filter and linear feedback. A parametric study shows that suitable combinations of plant and sensor noise characteristics, and state weighting matrices can be selected to meet the mission RMS pointing requirements. The effect of removing the hoop-mounted actuator is to cause an increase in the RMS errors along with the increased control effort. An increase in least damped modal time constant is also noted, when the hoop-mounted actuator is removed. The effect of removing the hoop-mounted sensor is to cause an increase in the RMS errors along with the degradation in the estimator performance. However, removing the hoop-mounted actuator causes a greater degradation in the system RMS performance than removing the hoop-mounted sensor.


## I. Introduction

Orbiting large flexible space structures have been considered for use in future large scale communications and other fields. As the size of the spacecraft system increases and the ratio of weight to area decreases, flexibility considerations become very important. This is in contrast to small space structures which are assumed to be rigid. One such large flexible space structure which has been proposed for future space missions is the Hoop/Column Antenna System which is depicted in Fig. 1 in its deployed configuration.

The Hoop/Column system[1], contains a deployable (telescoping) mast system connected to the hoop by support cables under tension. The hoop contains 48 rigid sections to be deployed by motor drive units.

The desired shape of the RF reflective mesh is produced by a secondary drawing surface using control cables. The reflective mesh is connected to the hoop by quartz or graphite stringers. At one end of the mast the electronic feed assemblies are positioned, whereas at the other end are the principal solar arrays connected to the main bus based control. In order to achieve the required RF performance a pointing accuracy of $\pm$(0.03-0.10) degrees RMS and a surface accuracy of 12mm RMS will be required. A finite element model of the Hoop/Column structural system without damping, is taken as the basis for the controls analysis. In order to reduce the dimensionality of the system, for computational ease, a modal transformation is carried out. In this case the truncated system contains thirteen modes, comprising the six rigid translational and rotational modes and the first seven flexible modes.

The controls analysis of the Hoop/Column antenna system requires specification of the types of actuators and their locations and orientations in the structure. For this study point thrusters and torquers are assumed to generate the required control forces and torques. Since we are considering thirteen modes, it is convenient here to choose a maximum of thirteen actuators in this analysis. Controllability and observability considerations of the Hoop/Column system based on the proposed location of actuators as shown in Fig. 2 have been established using graph theoretic techniqes.[2]

An optimal control law is realized by combination of the Kalman filter and linear feed-back techniques (Fig. 3). The controls analysis is carried out assuming collocated and noncollocated sensors and actuators. The plant and sensor noises are assumed to be uncorrelated, zero-mean white Gaussian processes.

## II. Mathematical Formulation of the Problem

The dynamic model of the Hoop/Column structural system in the absence of damping can be represented as[3],

$$M\ddot{Z} + KZ = F_c \qquad (1)$$

where

M - 6n x 6n mass/inertia matrix

K - 6n x 6n stiffness matrix

Z - 6n x 1 matrix consisting of the displacements and rotations at the nodal points

$F_c$ - 6n x 1 control vector.

$$F_c = B_c U \qquad (2)$$

where

$B_c$ - control influence matrix of order 6n x p

for

p - number of actuators

U - p x 1 matrix associated with the control vector.

In the present model represented by Eq. (1) the number of nodes is equal to 112 (i.e. n = 112), corresponding to the number of nodal (grid) points in the FEM output and the number of actuators is equal to 13 (or 12).

To decrease the dimensionality of the system a modal transformation is carried out defining

$$Z = \Phi q \tag{3}$$

where $\Phi$ is the matrix containing the eigenvectors of Eq. (1) and is of order (6n x m), for m number of modes and q is a modal vector of order (m x 1). In this case, m = 13.

After using the transformation, Eq. (3), in Eq. (1) there results

$$\Phi^T M \Phi \ddot{q} + \Phi^T K \Phi q = \Phi^T F_c \tag{4}$$

The left hand side of Eq. (4) can be rewritten, using the properties of the eigenvalues and associated eigenvectors as

$$[\,m_i\,]\,\ddot{q} + [\,K_i\,]\,q = \Phi^T F_c \tag{5}$$

where

$$\Phi^T M \Phi = \text{diag}\,[\,m_i\,] = [\,m_i\,],\ i = 1,2..13$$

$$\Phi^T K \Phi = \text{diag}\,[\,K_i\,] = [\,K_i\,],\ i = 1,2..13$$

Eq. (5) can be rewritten in the form

$$\dot{X} = AX + BU \tag{6}$$

where

$$X = \begin{bmatrix} q_1 \\ q_2 \end{bmatrix} \qquad A = \left[\begin{array}{c|c} 0 & I \\ \hline -[\,m_i\,]^{-1}\,[\,K_i\,] & 0 \end{array}\right]$$

and

$$B = \begin{bmatrix} 0 \\ \hline [\, m_i \,]^{-1}\, \phi^T B_c \end{bmatrix}$$

The plant noise, w, may be incorporated into Eq.(6) to model the stochastic linear dynamic system of the form:

$$\dot{X} = AX + BU + Gw \tag{7}$$

The measurements, Y, are assumed to be related to the state through the observation matrix, H, and the measurement noise, v, by

$$Y = HX + v \tag{8}$$

Eqs. (7), (8), along with the cost function

$$J = \lim_{t_f \to \infty} \{E\,[X^T(t_f)Q_f X(t_f)] + \int_{t_0}^{t_f} (X^T Q X + U^T R U)\,dt]\} \tag{9}$$

completely define the stochastic problem.[4] The minimization of the cost function yields the optimal control vector, U, obtained from

$$U = -C\,\hat{X} \tag{10}$$

where $\hat{X}$ is the state estimate, and

$$C = R^{-1}B^T K_1 \tag{11}$$

where $K_1$ is the steady state solution of the matrix Riccati differential equation,

$$-\dot{K}_1 = K_1 A + A^T K_1 - K_1 B R^{-1} B^T K_1 + Q \tag{12}$$

The state estimate $\hat{X}$, is obtained, from [5]

$$\dot{\hat{X}} = A\hat{X} + BU + F\,(Y - H\hat{X}) \tag{13}$$

with the filter gain, F, expressed as

$$F = PH^T V^{-1} \tag{14}$$

where, P is the steady state solution of the filter matrix Riccati equation:

$$\dot{P} = AP + PA^T - PH^T V^{-1} HP + GWG^T \tag{15}$$

with

$$W\,\delta\,(t-T) = E[w(t)w^T(T)] \tag{16}$$

and

$$V\,\delta(t-T) = E[v(t)v^T(T)] \tag{17}$$

Substitution of Eq. (10) into Eq. (7) and Eqs. (8) and (10) into Eq. (13) will yield the following differential equations which could be used for simulation of stochastic optimal control systems (Fig. 3).[6]

$$\dot{X} = AX - BC\hat{X} + Gw \tag{18}$$

$$\dot{\hat{X}} = (A - FH - BC)\hat{X} + FHX + Fv \tag{19}$$

## IIA. Simulation of the Steady State RMS State Components

After subtracting Eq. (18) from Eq. (19) a differential equation for the error results as follows:

$$\dot{e} = (A - FH)\,e + Fv - Gw \tag{20}$$

Furthermore, Eq. (19) can be rewritten as

$$\dot{\hat{X}} = (A - BC)\,\hat{X} - FHe + Fv \tag{21}$$

The covariance of the reconstruction error, $P = E[ee^T]$, and the covariance of the state estimate, $\hat{X}_1 = E[\hat{X}\hat{X}^T]$, can be obtained from Eqs. (20) and (21) as,

$$\dot{P} = AP + PA^T - PH^TV^{-1}HP + GWG^T \tag{15}$$

$$\dot{\hat{X}}_1 = (A - BC)\hat{X}_1 + \hat{X}_1(A - BC)^T + FVF^T \tag{22}$$

The covariance of X is given by

$$E[XX^T] = E[(\hat{X} - e)\,(\hat{X} - e)^T] = \hat{X}_1 + P \tag{23}$$

For the case when $\dot{P} \to 0$ and $\dot{\hat{X}}_1 \to 0$, the steady state variances of e and $\hat{X}$ and, hence, of X can be found.

## III. Possible Arrangement of Actuators for the Hoop/Column System

Out of the maximum of thirteen actuators selected twelve actuators consisting of point actuators and a torquer are assumed to be located at selected grid positions in the feed assembly as well as on the column, while the remaining actuator is assumed to be a point actuator mounted on one of the rigid links of the hoop assembly with thrust direction tangential to the hoop circle.

Table 1 indicates the relationship between the actuators and the modes they directly influence, the frequency of each mode, the generalized mass and the generalized stiffness.

Table 1 - Relation between Actuators and Modes Directly Influenced

| Actuator No. (circled in Fig. 2) | Mode Affected ( ) | Frequency Hz | Generalized mass $m_i$ (lb-sec$^2$/in) | Generalized stiffness $k_i$ (lb/in) |
|---|---|---|---|---|
| 1,2,3, & 4 | Feed Mast Torsion (12) | 0.88976 | 723.522 | 22612.9 |
| 5 | First Bending (about Y axis) (8) | 0.214246 | 5.233 | 9.483 |
| 6 | First Bending (about X axis) (9) | 0.270956 | 3.073 | 8.907 |
| 7 | Surface Torsion (10) | 0.506323 | 0.305 | 3.083 |
| 8(Torquer) | Yaw (rot. about Z axis) and First Torsion (7) | 0.0 and 0.118835 | 8.419 & 153.157 | 0.0 & 85.385 |
| 9 | Transl. along X axis & Second Mast Bending (11) | 0.0 and 0.728873 | 16.444 & 1.993 | 0.0 & 40.887 |
| 10 | Transl. along Y axis & Second Mast Bending (13) | 0.0 and 0.919231 | 8.925 & 0.658 | 0.0 & 21.954 |
| 11 | Transl. along Z axis | 0.0 | 7.349 | 0.0 |
| 12 | Pitch (rot. about Y axis) | 0.0 | 2.941 | 0.0 |
| 13 | Roll (rot. about X axis) | 0.0 | 9.704 | 0.0 |

NOTE: If there is more than one numerical value in any column, the first one corresponds to a rigid mode while the second corresponds to the flexible mode, respectively.

## IV. Numerical Simulation and Synthesis of Control Law

For the proposed arrangement of actuators in the structure, a parametric study was performed showing the effect of varying the state penalty matrix Q (from 100I to 10000I) and the control penalty matrix, R(from I to 100I) on the least damped mode of the system (Fig. 4). It has been concluded that Q = 1000I, R = I is a suitable design point from the stand point of minimizing the least damped modal time constant and maintaining a reasonable control effort.[3] Further, the stability of the closed-loop system, consisting of the plant and the estimator, has been established for all combinations of parameters considered in this study.[7]

Plant noise covariances ranging from 0.00001 I(26 x 26) to 0.0000001 I(26x26) and sensor noise covariances ranging from 0.0000025 I(13 x 13) to 0.00025 I(13 x 13) are assumed in the analysis. Selection of the range of plant noise covariances in the modal coordinates is based upon plant noise intensity ranging from $1 \times 10^{-6}$ to $1 \times 10^{-8}$ (lb-m).[2] Selection of the range of sensor noise covariances in the modal coordinates is based upon sensor noise intensities in the range of $1 \times 10^{-5}$ to $1 \times 10^{-7}$ [(rad)$^2$ or (rad/sec)$^2$, etc].[8] Based on the accompanying analysis, it is seen that the estimated modal coordinates closely follow the actual modal coordinates, thus ensuring a good estimation process.[7]

In this study, initial displacements of 0.01 are assumed in all the modal coordinates, which correspond to the expected maximum allowable perturbations in the linear range from the nominal operating required RMS displacements; these amplitudes for the modal displacements are obtained through calculation of Eq. (3).

Numerical studies show that when noise is included in the model that increasing the elements of the state weighting matrix by an order of magnitude increases the control effort required by an order of magnitude, but does not cause a significant improvement in the system response.[7] (But, it was found in the deterministic case that increasing the elements of the state weighting matrix causes a significant improvement in the system response.[3])

A further parametric study was conducted to determine the range of system parameters which meet the mission RMS pointing accuracy requirements. Fig. 5 shows the relationship between the steady state RMS pointing errors (in some of the modal coordinates) and the state weighting matrices, for initially assumed noise covariances of W = 0.00001 I(26 x 26) and V = 0.0000025 I (13 x 13).

Fig. 5 shows a similar relationship for plant and sensor noise covariances of W = 0.0000001 I(26 x 26) and V = 0.00025I(13 x 13), respectively. A comparison of Fig. 5 with Fig. 6 reveals that there is a decrease in the magnitude of the RMS errors in the latter case, for all values considered for the steady state weighting matrix elements. In addition, the steady state RMS errors, for almost all numerical combinations of the elements of the state weighting matrix and of the noise covariance matrix considered in Fig. 6, are within the allowable maximum as specified by the mission requirements; as a contrast some of the RMS errors shown in Fig. 5 would actually exceed the mission specifications. [It is also important to note that the range of maximum actuator force amplitudes is about the same in both the cases.[7]]

In a recent related study[3], it was found that the hoop-mounted actuator plays an important role in controlling the system. In this analysis, the effect of removing the hoop-mounted actuator (whose thrust direction is assumed to be tangential to the hoop circle) is to cause a deterioration in the least damped modal time constants. The range of the maximum force amplitudes required, in response to initial displacements of 0.01 in all the modes, is also increased (Table 2). Further, amplitudes of the RMS pointing errors are increased substantially in all the coordinates as compared to the case where all 13 actuators are present, as can be seen by comparing Fig. 7 with Fig. 5.

The effect of removing the hoop-mounted sensor is to cause a deterioration in the least damped time constant associated with the estimator poles, thus degrading the estimator dynamics. There appears to be a redistribution and a small increase in the RMS errors as is evident by comparing Fig. 8 with Fig. 5.

In another recent related study[9], only torque actuators located on the mast are considered for controlling the antenna attitude and flexible motions (using LQG theory as well as other techniques). However, it was suggested that hoop-mounted control devices might be effective in controlling certain torsional modes, which is made clear in our study. It should be kept in mind that the problems related to the design of control hardware remain yet to be answered.

## V. Conclusions

Control system synthesis is considered here for a large space antenna system and is based on stochastic linear optimal control techniques. From this preliminary analysis, it appears that the performance requirements can be met by using linear quadratic Gaussian techniques. Parametric studies show that suitable combinations of plant and sensor noise characteristics, and state weighting matrices can be selected to meet the mission RMS pointing requirements; here a definite trade-off exists between the increased complexity, cost, weight, and reliability of the system, and the possible gain in the system performance.

Table 2

Comparison of Maximum Actuator Force Amplitudes

$Q = 10001$, $R=I$, $q_i(0)=0.01$, $i=1,2\ldots,13$

13 Modes

$W = 0.00001$, $V = 0.0000025$

| Maximum actuator force amplitudes (pounds) | 13 Actuators 13 Sensors | 13 Actuators 13 Sensors |
|---|---|---|
| $f_1$ | 0.3330 | 2.3548 |
| $f_2$ | 0.0570 | 0.0453 |
| $f_3$ | 0.2681 | 2.2954 |
| $f_4$ | 0.0570 | 0.0453 |
| $f_5$ | 1.3028 | 1.3024 |
| $f_6$ | 0.2865 | 0.5520 |
| $f_7$ | 1.2310 | ------ |
| $f_8$ (in-lb) | 0.0140 | 0.0644 |
| $f_9$ | 0.2859 | 0.5328 |
| $f_{10}$ | 0.1574 | 0.1694 |
| $f_{11}$ | 0.4086 | 0.3693 |
| $f_{12}$ | 0.3521 | 0.3521 |
| $f_{13}$ | 0.0660 | 0.0993 |

The effect of removing the hoop-mounted actuator is to cause an increase in the RMS errors along with the increased control effort. An increase in the least damped modal time constant is also noted, when the hoop-mounted actuator is removed. [It is interesting to note that removing the hoop-mounted actuator resulted in an increased control effort and also increased the least damped modal time constant, in the deterministic study also.[3]] The effect of removing the hoop mounted sensor is to cause an increase in the RMS errors along with the degradation in the estimator performance.

In order to arrive at more complete conclusions, factors such as time delay, and nonlinearities in the plant and sensors should be considered. Since many of the current (and proposed) sensor systems provide data in a discontinous (discretized) format, another suggestion is to reformulate the current analysis in a discretized time basis.

## References

1. Sullivan, M.R., "Maypole (Hoop/Column) Concept Development Program," Large Space Systems Technology - 1981, Third Annual Technical Review, NASA Langley Research Center, Nov. 16-19, 1981, NASA Conference Publication 2215, Part 2, pp. 503-550.

2. Reddy, A.S.S.R. and Bainum, P.M., "Controllability of Inherently Damped Large Flexible Space Structures," Acta Astronautica, Vol. 10, No. 5-6, 1983, pp. 357-363.

3. Bainum, P.M. and Reddy, A.S.S.R., "On the Controllability and Control Law Design for a Large Flexible Antenna System," 34th International Astronautical Congress, Budapest, Hungary, Paper No. 83 - 340, Oct. 10-15, 1983.

4. Gelb, A.E., (Editor) Applied Optimal Estimation, The M.I.T. Press, Massachusetts Institute of Technology, Cambridge, Massachusetts, 1974, pp. 356-365.

5. Bryson, A.E. and Ho, Y.C., Applied Optimal Control, Blaisdell Publishing Co., Waltham, Massachusetts, 1969, pp. 414-418.

6. Armstrong, E.S., ORACLS - A Design System for Linear Multivariable Control (Volume 10), Marcel Dekker Inc., New York 1980.

7. Ananthakrishnan, S., "Stochastic Optimal Control of a Large Flexible Space Antenna," Master's Thesis, Dept. of Mechanical Engineering, Howard University, Washington, D.C. 20059, July 1984.

8. DeLorenzo, M.L., "Selection of Noisy Sensors and Actuators for Regulation of Linear Systems," Purdue University, School of Aeronautics and Astronautics, West Lafayette, Indiana 47907. Technical Report, Grant AFOSR 82-0209.

9. Joshi, S.M., "Control System Synthesis for a Large Flexible Space Antenna," XXXIIIrd Congress of the International Astronautical Federation, Paris, France, Sept. 26th - Oct. 2, 1982, Paper No. 82-320.

Acknowledgement

Research partly supported by NASA Grant NSG-1414 and the NASA/ Howard Univ. Large Space Structures Institute.

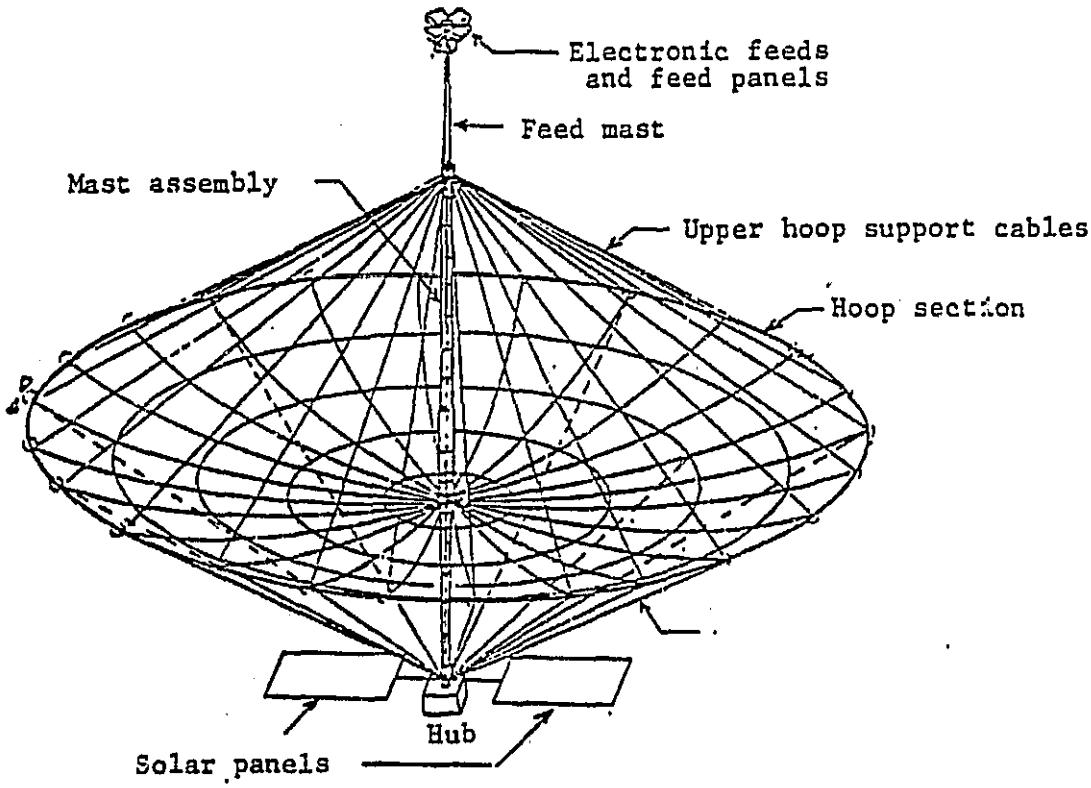


Fig. 1. The Hoop/Column Antenna System.

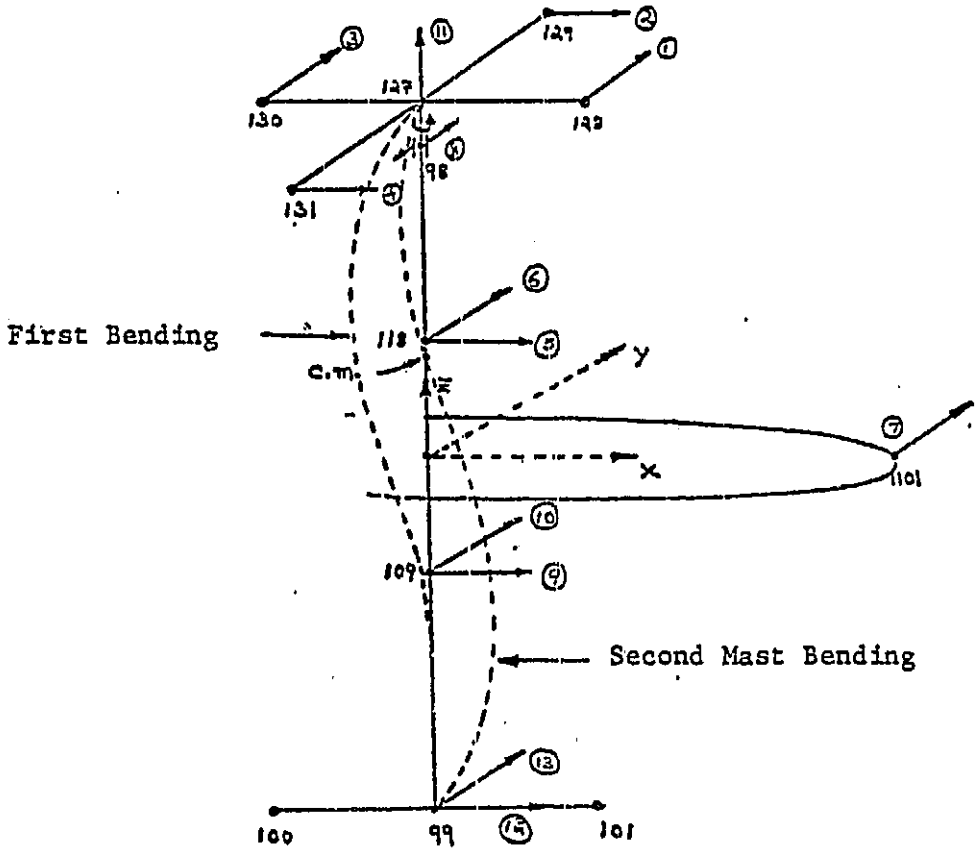


Fig. 2. Proposed Arrangement of Actuators-Hoop/Column System (uncircled numbers identify grid points from finite element analysis).

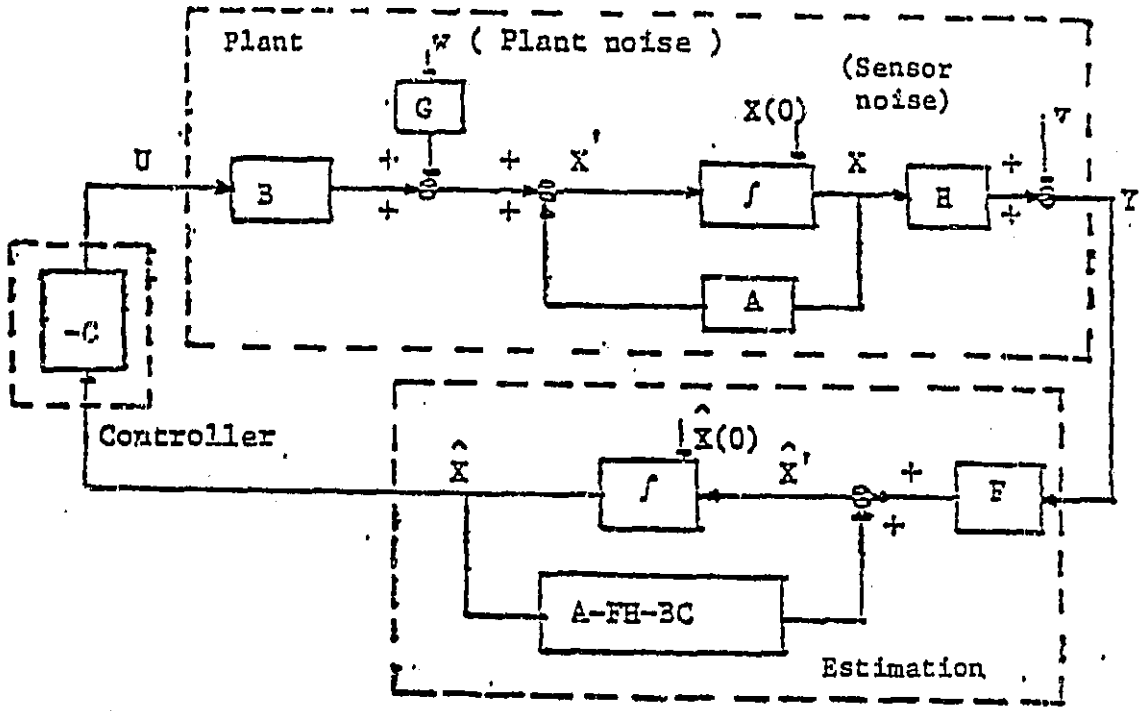


Fig. 3. Stochastic Optimal Control Configuration.

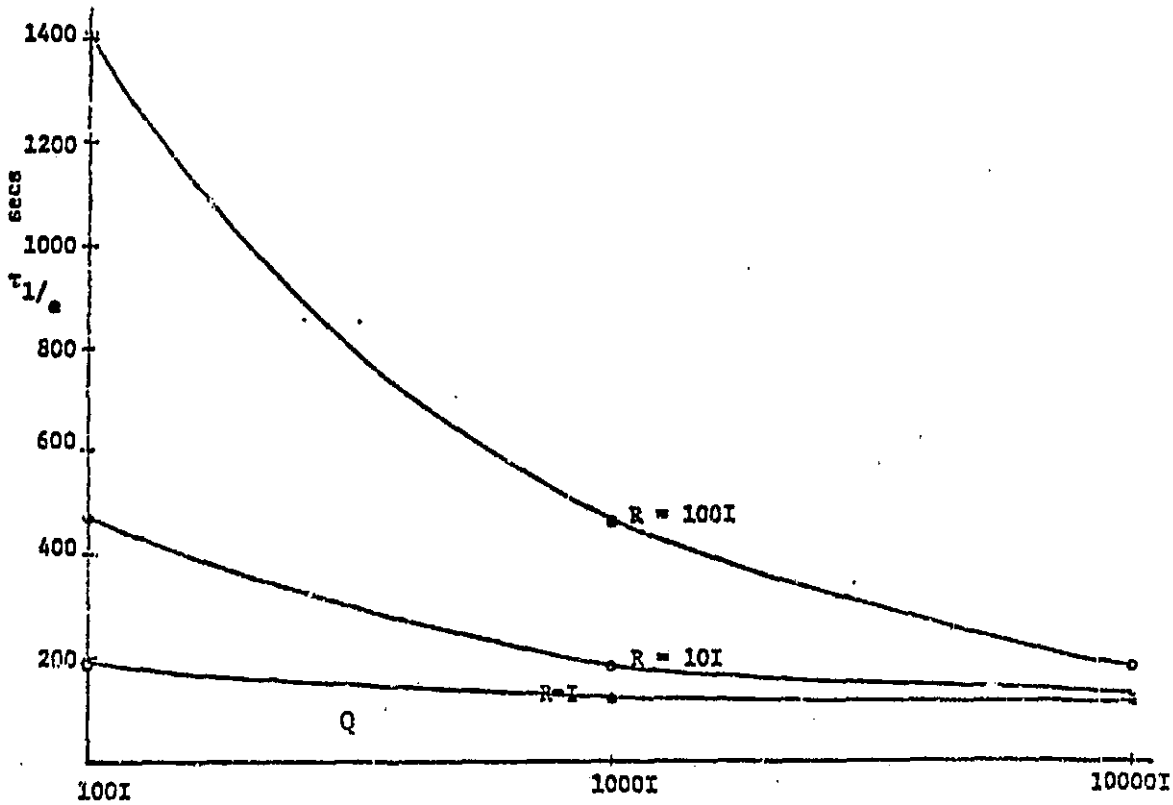


Fig. 4. Variation of the Time Constant of the Least Damped Mode with Q and R Penalty Matrices.

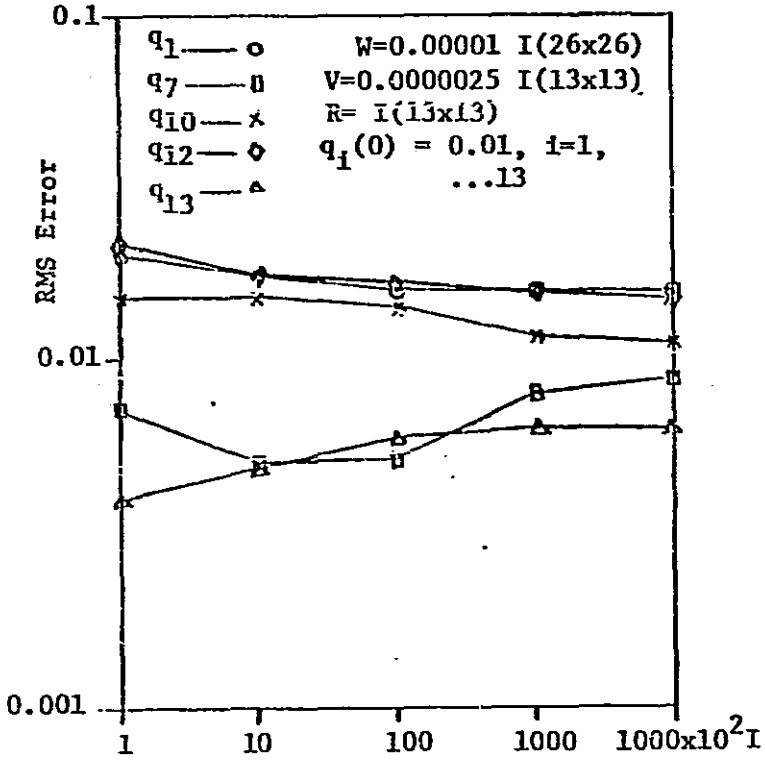


Fig. 5. Steady State RMS Errors in Selected Modal Coordinates for Collocated Actuators and Sensors 13 Actuators/ 13 Sensors/ 13 Modes.

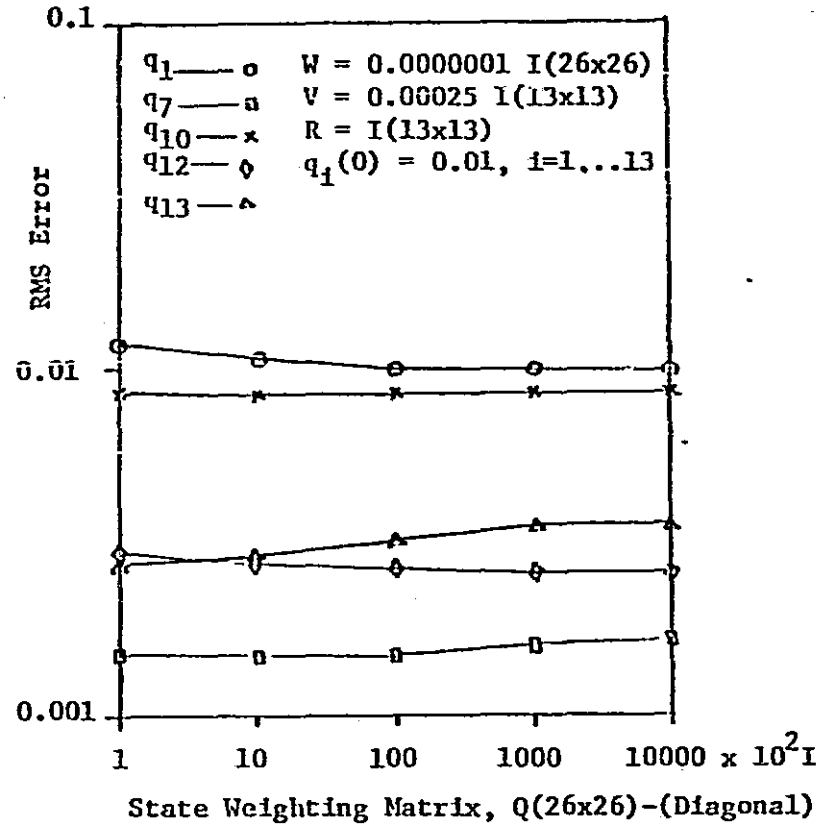


Fig. 6. Steady State RMS Errors in Selected Modal Coordinates for Collocated Actuators and Sensors - 13 Actuators/13 Sensors/ 13 Modes - Effect of Further Decreasing W and Increasing V.

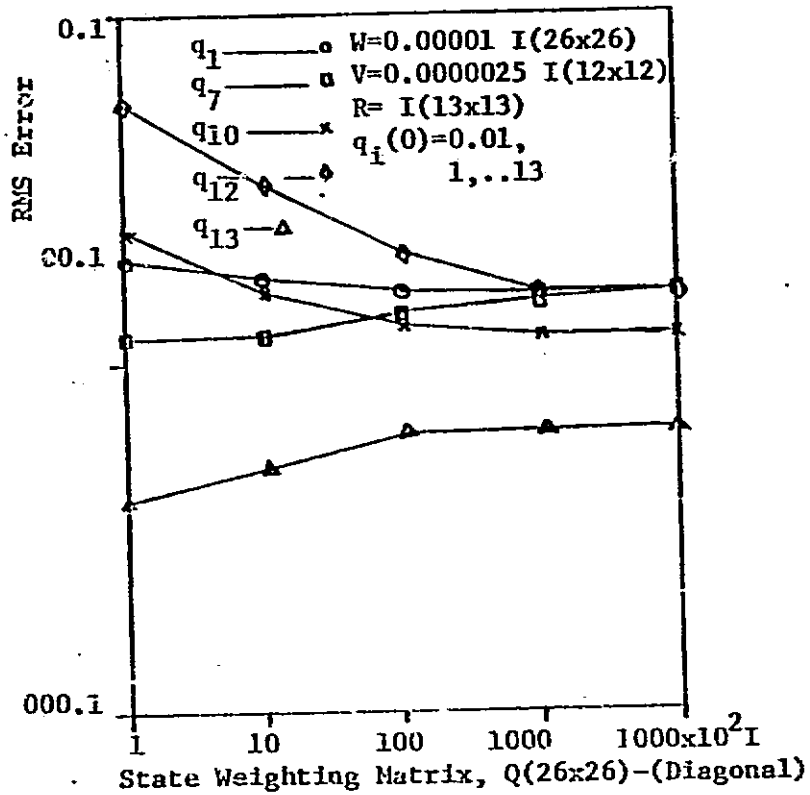


Fig. 7. Steady State RMS Errors in Selected Modal Coordinates for Non-Collocated Actuators and Sensors - 12 Actuators/13 Sensors/13 Modes (Hoop-Mounted Actuator Removed).

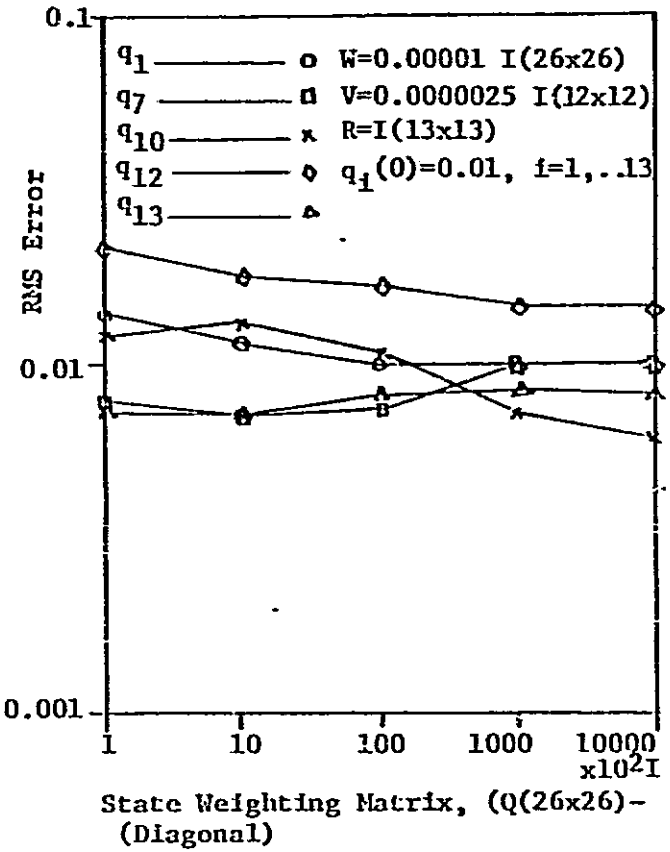


Fig. 8. Steady State RMS Errors in Selected Modal Coordinates for Non-Collocated Actuators and Sensors - 13 Actuators/ 12 Sensors/ 13 Modes (Hoop-Mounted Sensor Removed).

## V. CONCLUSIONS AND RECOMMENDATIONS

A two dimensional model of the SCOLE configuration open-loop dynamics has been developed and will provide the basis for the modelling of the three dimensional dynamics wich has already been initiated. Calculation of open-loop appendage frequencies is seen to be dependent on the boundary conditions assumed at both the Shuttle and the reflector ends of the mast, and also somewhat dependent on whether a (decoupled) continuum or (coupled) finite element model is used to model the appendage modes. The Floquet stability analysis, initiated during this reporting period, should provide considerable insight into possible parametrically induced open-loop instabilities which should be understood prior to the design of the control system.

Numerical examples illustrate the potential instabilities that could result for large ordered systems (typical of LSST) even with input delays that are only a small fraction of the system's frundamental open-loop period. Such delays could be associated with actuators or other system hardware. This work should be extended to analyze the effects of input delays which could be associated with the SCOLE in-orbit or laboratory test scale model configurations.

A parametric study of a stochastic closed-loop linear system dynamic model of the Hoop/Column system shows that suitable combinations of plant and sensor noise characteristics and LQG state and control weighting matrix elements can be selected to meet the mission RMS pointing and antenna shape accuracy requirements.

The important role of a hoop-mounted actuator in reducing RMS errors as well as improving the transient response characteristics, especially in the torsional type modes should be noted. Failure of the hoop-mounted sensor could result in an increase in RMS errors and also a degradation in the estimator performance.